Ana Elisa Ribeiro Orsi

Evaluation of *in vitro* models for the study of human X chromosome inactivation

Avaliação de modelos *in vitro* para o estudo da inativação do cromossomo X em humanos

São Paulo

2023

Ana Elisa Ribeiro Orsi

Evaluation of *in vitro* models for the study of human X chromosome inactivation

Avaliação de modelos *in vitro* para o estudo da inativação do cromossomo X em humanos

Dissertação apresentada ao Instituto de Biociências da Universidade de São Paulo, para a obtenção de Título de Mestre em Ciências, na Área de Biologia/Genética.

Orientadora: Profª. Drª. Lygia da Veiga Pereira
Co-orientador: Prof. Jun Wu

São Paulo

2023

Ficha catalográfica elaborada pelo Serviço de Biblioteca do Instituto de Biociências da USP,
com os dados fornecidos pelo (a) autor (a) no formulário:
'https://biblioteca.ib.usp.br/ficha-catalografica/src/ficha.php'

Ribeiro Orsi, Ana Elisa
Avaliação de modelos in vitro para o estudo da inativação do cromossomo X em humanos / Ribeiro Orsi Ana Elisa ; orientadora da Veiga Pereira Lygia -- São Paulo, 2023.
63 p.

Dissertação (Mestrado) -- Instituto de Biociências da Universidade de São Paulo. Programa de Pós-Graduação em Ciências Biológicas (Biologia Genética).

1. Inativação do cromossomo X. 2. Células tronco pluripotentes. 3. Blastoides. I. da Veiga Pereira, Lygia, orient. Título.

Bibliotecária responsável pela catalogação:
Elisabete da Cruz Neves - CRB - 8/6228

Comissão Julgadora:

_____ _____

Prof(a). Dr(a). Prof(a). Dr(a).

_____ _____

Prof(a). Dr(a). Profª. Drª. Lygia da Veiga Pereira

Orientadora

Acknowledgements

I thank my advisors, prof. Lygia da Veiga Pereira Carramaschi and prof. Jun Wu, for providing extensive support and meaningful discussions throughout the development of this work.

I thank the members of my Master's committee, professors Edroaldo Lummertz da Rocha, Irene Yan and Maria Vibranovski, for the valuable insights and support provided.

I thank Carlos Pinzón-Arteaga, not only for teaching me wet lab techniques, but also for serving as a role model of how to thrive in the academic environment. This work would have not been possible without you.

I thank all the colleagues who have been with me in this journey, for your friendship and support: Rayssa, Cláudia, Raquel, Fabiano, Daniel, Alexandre, Rodrigo, Yordanka and Patricia in Brazil, Lin, Anna, Emily, Menaka, Lizhong, Seiya, Yingying, Daniel, Jia, Bingbing, Saku, Yi Ding, Mechi, James, Eunice and Yi Peng in the US.

I thank prof. Wei Jiang, for sharing single-cell RNA-seq data of EPSCs and ESCs, and prof. Thorold Theunissen, for providing the WIBR3 MECP2-GFP/tdTomato cell line used throughout this work.

I thank my family for the incentive and support. Thank you for patiently listening to my constant talks about calico cats, dividing cells, embryos and more.

I thank Marco for standing by my side this whole time.

I thank the staff of the Institute of Biosciences of the University of São Paulo and the Molecular Biology department of UTSW for the technical and administrative support.

Finally, I thank CAPES and FAPESP (processes 2020/16612-9 and 2022/02096-4) for providing financial support for this project.

Resumo

A inativação do cromossomo X (ICX) é um processo de compensação de dose que ocorre nas células fêmeas de mamíferos placentários. A ICX em humanos inicia-se por volta do estágio de blastocisto, e seu entendimento é prejudicado pelas dificuldades associadas ao uso de embriões em pesquisa. Para lidar com esse problema, nós avaliamos diferentes modelos para o estudo da ICX *in vitro*. Células no estado primed exibiram expressão monoalélica do gene *MECP2*, ligado ao cromossomo X, e uma única nuvem de *XIST*. Após conversão para o estado naive, expressão bialélica do gene *MECP2* foi observada, assim como a ausência de nuvens de *XIST* durante as primeiras duas passagens. Avaliação de EPSCs *in vitro* e *in silico* sugeriram que essas células já passaram pelo processo de ICX. Resultados similares foram observados para células cultivadas no meio 4CL. Depois de nova conversão para o estado primed, células naive cultivadas em 5iLA passaram pela inativação do mesmo alelo do gene *MECP2* previamente inativo. Por outro lado, blastoides gerados a partir de células cultivadas no meio PXGL demonstraram ICX progressiva e aleatória, apesar de viés para re-inativação do alelo de *MECP2* previamente inativo ter sido observado. Esses resultados sugerem que blastoides humanos podem ser usados para o estudo da ICX humana *in vitro*.

Abstract

X chromosome inactivation is a dose compensation mechanism that takes place in the cells of female placental mammals. Human XCI starts around the early blastocyst stage, and its understanding is hampered by the difficulties associated with the use of embryos in research. In order to address this issue, we evaluated different models for the study of XCI *in vitro*. Primed cells displayed monoallelic expression of the X-linked gene *MECP2* and a single *XIST* cloud. Upon conversion to the naive state, biallelic *MECP2* expression was observed, as well as absence of *XIST* clouds for the first two passages. Evaluation of EPSCs *in vitro* and *in silico* suggests that these cells have already undergone XCI. Similar results were observed for cells cultured in 4CL medium. After repriming, naive cells cultured in 5iLA displayed inactivation of the previously inactive *MECP2* allele. On the other hand, blastoids generated from cells cultured in PXGL underwent progressive random XCI, although bias for the previously inactive allele was still observed. These results suggest that blastoids could be potentially employed for the study of human XCI *in vitro*.

List of Figures

List of Tables

List of Abbreviations

aPKC: Atypical protein kinase C
BMP: Bone morphogenetic protein
BSA: Bovine serum albumin
CET: Chroman 1, Emricasan, and Trans-ISRIB
CT: Cytotrophoblast
DiM: (S)-(+)-dimethindene maleate
EGA: Embryonic genome activation
EPG: Epidermal growth factor
EpiSCs: Epiblast stem cell
ERK: Extracellular signal-regulated kinases
ESC: Embryonic stem cell
FBS: Fetal bovine serum
FGF: Fibroblast growth factor
GFP: Green fluorescent protein
GSK3: Glycogen synthase kinase-3
HDM: Hypoblast differentiation medium
ICM: Inner cell mass
IPSC: Induced pluripotent stem cell
JNK: Jun N-terminal kinase
LIF: Leukemia inhibitory factor
MAPK: Mitogen-activated protein kinase
MECP2: Methyl-CpG binding protein 2
MEF: Mouse embryonic fibroblasts
MEK: MAPK/ERK kinase
MiH: Minocycline hydrochloride
PARP: Poly-ADP ribose polymerase
PBS: Phosphate buffered saline
PFA: Paraformaldehyde
PSC: Pluripotent stem cell
RNA-FISH: RNA fluorescence in situ hybridization
ROCK: Rho-associated protein kinase
scRNA-seq: Single-cell RNA sequencing
SNP: Single nucleotide polymorphism
TDM: Trophoblast differentiation medium
TRITC: Tetramethylrhodamine iso-thiocyanate
TSC: Trophoblast stem cell
XCI: X chromosome inactivation
XCR: X chromosome reactivation
XIC: X inactivation center
XIST: X-inactive specific transcript
8CLC: 8 cell-like cell

Index

1 - Introduction

1.1 - X chromosome inactivation

In the human species, as well as the other placental mammals, the allosomes are responsible for sex determination. The male and female biological sexes are determined by the presence of XY and XX genotypes, respectively. The X chromosome is long and houses genes related to vision, blood coagulation and other functions common to both sexes (ROSS et al., 2005). By inheriting two copies of this chromosome, females present twice as many copies of X-linked genes as males. The imbalance is solved by the process of X chromosome inactivation (XCI), a biological mechanism which assures the inactivation of exceeding copies of the X chromosome in every somatic cell of the body (KAUR; RV; GAYEN, 2019).

Initial studies about XCI were conducted in the mid-twentieth century, and employed mice and house cats as models. Barr and Bertram (1949) located a distinct structure in the perinuclear region of female, but not male, cells. The object was denominated “Barr body” and was subsequently identified in other mammal cells, including human blastocyst-stage blastomeres (PARK, 1957). It was later suggested that the structure could correspond to a condensed X chromosome (OHNO; KAPLAN; KINOSITA, 1959). This hypothesis was later tested by Mary Lyon, through the observation of coat color in mice, a trait determined by X chromosome-linked genes. Previously, it had been suggested that the female-specific multicolor coat patterns, such as tortoiseshell and mottled, were caused by specific alleles. Instead, Lyon proposed that random inactivation of one of the alleles of the X-linked gene that determines coat color in heterozygous individuals could explain the observed inheritance pattern (LYON, 1961). Her hypothesis was later found to be correct (LYON, 1999).

In turn, the inactivation of one of the copies of the X chromosome generates a different imbalance: in comparison to the autosomes, present in pairs, there would be a single copy of the X chromosome available for transcription in each cell. Therefore,

in 1967, Ohno suggested that the active X chromosome in male and female cells would be overexpressed, overcoming the difference between allosomes and autosomes (OHNO, 2013). Although this idea remains controversial, Ohno's hypothesis has been corroborated by studies conducted in different organisms, including humans (DENG et al., 2011; LARSSON et al., 2019).

Not all X-linked genes, however, seem to be subject to XCI. This idea was first proposed as a hypothesis to explain the abnormal phenotypes of individuals with 45, X (Turner syndrome) and 47, XXY (Klinefelter syndrome) karyotypes (LYON, 1962). Escape from X chromosome inactivation is estimated to affect 15 to 30% and 3 to 7% of human and mouse X-linked genes, respectively (CARREL; WILLARD, 2005, BALATON; COTTON; BROWN, 2015; BERLETCH et al., 2015; TUKIAINEN et al., 2017). In both species, XCI escape has been shown to vary between tissues and individuals (BERLETCH et al., 2015; TUKIAINEN et al., 2017). In humans, most escapees are located in clusters scattered across the p arm of the chromosome, as well as in the pseudoautosomal region PAR1 (CARREL et al., 1999; BALATON; COTTON; BROWN, 2015; TUKIAINEN et al., 2017). Genes that variably escape XCI seem to be preferentially located in the boundaries of XCI escaping domains (BALATON; COTTON; BROWN, 2015)

The molecular mechanisms of XCI have been studied for over three decades. Initially, the analysis of deletions in X chromosomes incapable of undergoing XCI and translocations that caused partial XCI led groups to define an X chromosome-linked region sufficient for XCI induction, denominated X inactivation center (XIC) (RASTAN; ROBERTSON, 1985; BROWN et al., 1991a). Soon after, Brown et al. (1991b) identified a long non-coding RNA encoded in the XIC and exclusively expressed from the inactive X chromosome. The gene, denominated X-inactive specific transcript (*XIST*), was also described in the mouse and was subsequently shown to co-localize with the inactive X chromosome copy in the nucleus (BROWN et al., 1991b; BROWN et al., 1992). It was later demonstrated that disruption of a single *Xist* allele caused skewed inactivation of the wild-type chromosome, suggesting that *Xist* regulates XCI in cis (PENNY et al., 1996). This hypothesis was corroborated by Wutz and Jaenisch (2000), who showed that the

inducible expression of an *Xist* transgene in autosomes led to their transcriptional repression.

Ever since *XIST*'s discovery, several other genes located in the mouse XIC have been associated with XCI initiation and maintenance. For instance, the long non-coding RNA *Tsix* partially overlaps *Xist*, but is transcribed antisense to it. Besides coating active X chromosome copies, its deletion induces constitutive XCI in cis, suggesting a role in XCI inhibition (LEE; DAVIDOW; WARSHAWSKY, 1999). More recently, chromatin folding analysis have revealed that the mouse XIC is composed of two topologically associating domains (NORA et al., 2012). The *Tsix* promoter is located in the same domain as *DXPas34* (DEBRAND et al., 1999) and *Xite* (OGAWA; LEE, 2003), elements whose transcription is required for *Tsix* expression. Similarly, the *Xist* promoter shares the second domain with its enhancers *Jpx* (TIAN; SUN; LEE, 2010) and *Ftx* (CHUREAU et al., 2010).

In the early 2000s, researchers described the process of XCI in mouse embryos (HUYNH; LEE, 2003; MAK, 2004; OKAMOTO, 2004). It was shown that, at the second embryonic day, the X chromosome of paternal origin is inactivated in all murine blastomeres (HUYNH; LEE, 2003; MAK, 2004). This process is denominated imprinted XCI, as opposed to the random XCI observed in adult placental mammals. Later, at the blastocyst stage, the paternal inactive X chromosome is reactivated only in the inner cell mass cells. After that, a second, random, round of XCI takes place in the cells that will originate the embryo proper (MAK, 2004; OKAMOTO, 2004).

Although well described in the mouse, human XCI appears to be significantly different and has not been fully elucidated. The molecular mechanisms regulating the process, for instance, seem to greatly differ between the two species. *TSIX* is present in the human XIC, but does not seem to have a conserved role in XCI: the RNA is exclusively transcribed from the future inactive X chromosome copy, where it co-localizes with *XIST* (LEE; DAVIDOW; WARSHAWSKY, 1999; MIGEON et al., 2002). Instead, long non-coding RNA *XACT*, located outside the XIC, has been appointed as a more promising regulator of human XCI. *XACT* is expressed in pluripotent stem cells and during early development, coating active X chromosome copies in cis (VALLOT et al., 2013; VALLOT et al., 2017). In contrast to the mouse, *XIST* has been shown to coat both X chromosomes in human preimplantation female

embryos, as well as the male X chromosome (OKAMOTO et al., 2011; PETROPOULOS et al., 2016). Interestingly, although biallelic *XACT* expression is detected at the same stage, the two long non-coding RNAs are found to almost never co-localize. These observations suggest that *XACT* might compete with *XIST* during X chromosome coating, possibly decreasing its gene silencing effect (VALLOT et al., 2017).

Figure 1: Proposed XCI states of the early human embryo (A) and pluripotent stem cells (B) according to different hypotheses.

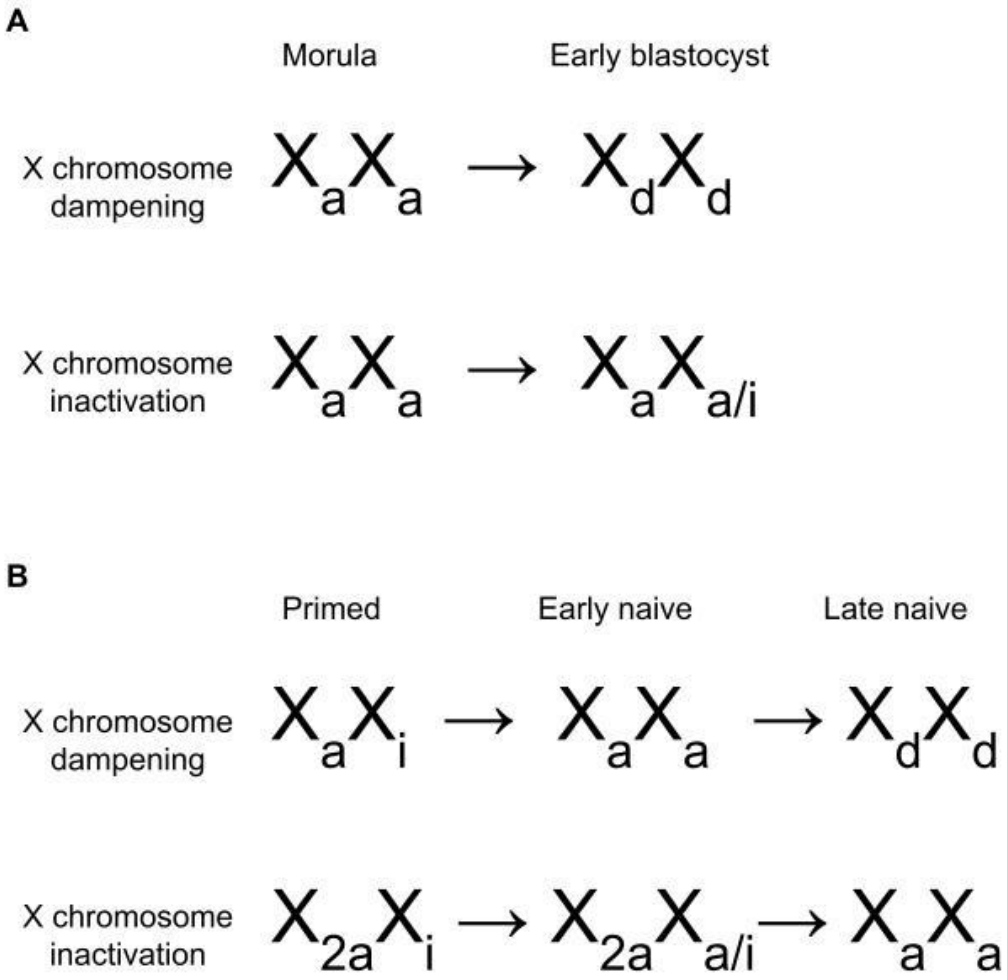

References: PETROPOULOS et al., 2016; MOREIRA DE MELLO et al., 2017; SAHAKYAN et al., 2017; MANDAL et al., 2020.

Differences between human and mouse XCI have also been identified in terms of progression during embryonic development. Petropoulos et al. (2016) sequenced

the transcriptomes of over 1500 cells from 88 embryos between developmental days 3 and 7. Through data analysis, the group did not see evidence of imprinted XCI in either embryonic or extraembryonic tissues, in accordance with previous reports (MOREIRA DE MELLO et al., 2010). They also concluded that, from the fourth day of development, both copies of the X chromosome in females were downregulated. The phenomenon, denominated dampening, would cause dosage compensation without complete inactivation of either X chromosome copy (PETROPOULOS et al., 2016) (Figure 1A).

Nevertheless, de Mello et al. (2017) proposed an alternative hypothesis to justify the group's results. Employing different strategies and analyzing additional sequencing data, the authors concluded that it was not possible to observe dampening in the sequenced cells: instead, XCI had started in the time points analyzed, but was not completed by developmental day 7, explaining the maintenance of biallelically expressed genes. Dosage compensation between the X chromosome and the autosomes was also assessed. It was shown that the process begins around the stages of morula and early blastocyst, but is not complete until the peri-implantation period (MOREIRA DE MELLO et al., 2017) (Figure 1A).

1.2 - Human preimplantation development

Human preimplantation development corresponds to the initial 7 days after fertilization. During the first 3 days, the zygote undergoes 3 successive cell divisions, originating 2, 4 and 8 cells. Between the second and third days, embryonic genome activation (EGA) takes place, and the synthesis of RNAs from the embryo’s genome is initiated. Next, on the fourth day, the embryo compacts, originating the morula. In this stage, the embryo's mass starts to increase, and cell divisions become faster (COTICCHIO et al., 2019). Around the fifth day, the blastocyst, characterized by the presence of a blastocoel cavity, trophectoderm and inner cell mass, is formed (SHAHBAZI, 2020).

The transition from morula to blastocyst is fundamental for embryonic development. Compaction is characterized by an increase in cell adhesion, which leads to the polarization of the outer cells and generates a concentration gradient in

the structure (RIETHMACHER; BRINKMANN; BIRCHMEIER, 1995; COTICCHIO et al., 2019). The hypertonicity caused by the accumulation of ions in the intracellular space induces liquid to infiltrate inside the morula, generating the blastocoel (WATSON; BARCROFT, 2001).

The process of compaction also promotes, for the first time during embryonic development, the emergence of different cell lines: internal cells of the morula, which will preferentially contribute to the inner cell mass, and external cells, trophectoderm precursors (MIHAJLOVIĆ; BRUCE, 2017). Internal cells are characterized by the presence of a centered nucleus and the absence of an organization pattern of cell structures. External cells, on the other hand, are polarized and their surface has access to the external medium. Their nuclei are located in the basal portion, and cell adhesion structures and rigid microtubules are present in the baso-lateral domains. The apical portion, in turn, displays dynamic microtubules and microvilli (COTICCHIO et al., 2019; MIHAJLOVIĆ; BRUCE, 2017).

In the mouse, multiple pathways have been described as important for the morula's maintenance and maturing. The E-cadherin, as well as α, β and γ catenines were identified as involved in the process of compaction (VESTWEBER; KEMLER, 1985; RIETHMACHER; BRINKMANN; BIRCHMEIER, 1995; PEREZ-MORENO; JAMORA; FUCHS, 2003). Through cellular adhesion, they allow for the polarization of outer cells (VESTWEBER et al., 1987; RIETHMACHER; BRINKMANN; BIRCHMEIER, 1995; PEREZ-MORENO; JAMORA; FUCHS, 2003). The E-cadherin also assures the impermeability of the cell junctions, acting in the blastocoel formation (ECKERT; FLEMING, 2008). The protein was also identified as present in the process of cell adhesion in the human morula (CAMPBELL et al., 1995).

In turn, the Hippo signaling pathway, initially described in the drosophila, mediates the differentiation of cell lineages (HARVEY; ZHANG; THOMAS, 2013; MIHAJLOVIĆ; BRUCE, 2017). Angiomotin is expressed in the inner blastomeres, where cell adhesion is intense, activating the Hippo pathway. This allows the phosphorylation of YAP by LATS, preventing its transportation to the nucleus and maintaining the expression of genes like *Oct4* and *Sox2*, essential for the development of the inner cell mass. Meanwhile, in the outer cells of the morula, the

PAR3-PAR6-aPKC system, associated with cell polarity, inhibits the pathway. This allows YAP to reach the nucleus, where it binds the TEAD transcription factors, activating the expression of genes such as *Cdx2* and *Gata3*, which induce differentiation to the trophectoderm lineage. Thus, outer cells tend to compose the trophectoderm, while inside blastomeres mainly contribute to the inner cell mass (MIHAJLOVIĆ; BRUCE, 2017; COTICCHIO et al., 2019).

1.3 - Pluripotent stem cells

Pluripotent stem cells are characterized by their self-renewal potential and the capacity to contribute to all three embryonic germ layers (DE LOS ANGELES et al., 2015). In 1981, two groups simultaneously established culture conditions for *in vitro* maintenance of embryonic stem cells derived from the murine epiblast (mESCs) (EVANS; KAUFMAN, 1981; MARTIN, 1981). The method had to be adapted for *in vitro* culture of human ESCs (hESCs), which was only achieved in 1998 (THOMSON, 1998). Still, differences were observed between mESCs and hESCs, including the organization in dome-shaped and flat colonies, respectively.

In 2006, Takahashi and Yamanaka showed that induced pluripotent stem cells (iPSCs) could be derived from mouse somatic tissues by retroviral transduction of factors *Oct3/4*, *Sox2*, *c-Myc*, and *Klf4* (TAKAHASHI; YAMANAKA, 2006). Shortly after, in 2007, two groups simultaneously derived EpiSCs, pluripotent stem cells obtained from mouse post-implantation epiblast. Unlike mESCs and mouse iPSCs, EpiSCs grew in large monolayer colonies, resembling hESCs. Additionally, it was noted that while EpiScs and hESCs depended on FGF and Activin/Nodal signaling, LIF signaling was a requirement for mESCs and mouse iPSCs (BRONS et al., 2007; TESAR et al., 2007).

A study from 2008 helped clarify the signaling requirements for establishment and maintenance of mESCs. Previously, mESCs had been cultured in a combination of LIF with either serum or bone morphogenetic protein (BMP). Ying and collaborators showed that serum and BMP acted downstream of the ERK1/2 pathway, preventing differentiation. As an alternative, inhibition of ERK1/2 by specific compounds, coupled with LIF, allowed mESC proliferation. The glycogen synthase

kinase-3 (GSK3) inhibitor CHIR99021 could be added to increase cell proliferation and viability (YING et al., 2008). Therefore, while hESCs and EpiSCs rely on FGF signaling for proliferation, inhibition of FGF and ERK1/2 signaling is essential for preventing differentiation of mESCs.

These results suggested that the morphological and signaling differences between hESCs and mESCs might not be simply species-specific, but could instead reflect different pluripotency states. Nichols and Smith (2009) proposed that mESCs and mouse iPSCs were found in a naive pluripotency state, corresponding to the immortalization of cells from the mouse ground state preimplantation epiblast. These cells did not present differentiation biases, could contribute to both teratomas and blastocyst chimeras, and female cells presented two active X chromosomes and underwent random XCI upon differentiation. On the other hand, hESCs, human iPSCs and EpiSCs would reflect the post-implantation epiblast, and were denominated primed. They could be characterized by variable differentiation biases, the capacity to contribute teratomas, but not blastocyst chimeras, and the presence of a single active X chromosome in female cells (NICHOLS; SMITH, 2009). If this hypothesis were correct, it would suggest that the primed and naive states were not specific to mice, but may also be replicated in other mammals. While hESCs presented the characteristics of primed pluripotent stem cells, it might be possible to transition them into the naive state.

The idea was further supported by an extensive analysis carried out in 2014, single-cell RNA sequencing (scRNA-seq) of mouse embryos and mPSCs were performed (BOROVIAK et al., 2014). The study revealed that naive mESCs resemble the preimplantation epiblast at E4.5, while primed EpiSCs clustered with the E5.5 postimplantation epiblast. Additionally, the authors showed that blastomere's ability to proliferate independently of ERK signaling is lost after implantation, supporting the hypothesis proposed by Nichols and Smith in 2009. (BOROVIAK et al., 2014).

Based on the previous knowledge about naive pluripotency, the first media for maintenance of naive human PSCs were successfully developed in 2014. Two different approaches were described simultaneously by Takashima et al. (2014) and Theunissen et al. (2014). Takashima's protocol required derivation of naive hPSCs by transient expression of *KLF2* and *NANOG* transgenes. After conversion, the t2iLGö

medium was sufficient for maintenance of naive hPSCs. In turn, the condition developed by Theunissen and collaborators was denominated 5iLA and could be directly used for naive conversion, without the need for transient transgene expression. Both media included a MEK inhibitor, a GSK3 inhibitor and LIF, as well as additional components (Table 1).

Despite effectively maintaining cells in an early epiblast-like state, chromosomal abnormalities have been associated with naive culture conditions, in particular 5iLA (THEUNISSEN et al., 2014). It has been suggested since that lessening MEK inhibition could protect cells against genomic instability without compromising the properties of naive pluripotency (DI STEFANO et al., 2018). In 2016, Pastor et al. also showed that human cells in 5iLAF and t2iLGö presented transcriptional, but not epigenetic, similarity with the preimplantation epiblast stage. While the oocyte and blastocyst stage methylomes are strongly correlated, naive cells display with very weak correlation to the embryonic stages analyzed due to genome-wide demethylation, including loss of imprinting (PASTOR et al., 2016).

Subsequently, new strategies for naive conversion were established. A small molecule screening carried out in 2016 determined that tankyrase inhibition by XAV939, in combination with LIF and inhibitors for MEK and GSK3, could directly induce human naive pluripotency (ZIMMERLIN, L. et al., 2016). A year later, a modified protocol introduced an initial 3-day “RESET” step for conversion, including histone deacetylase inhibitor valproic acid. Upon reset, naive cells were maintained in a medium containing inhibitors for MEK, tankyrase and aPKC, as well as LIF, denominated PXGL (Table 1). The strategy required few components and feeder-free culture was supported (GUO et al., 2017; BREDENKAMP et al., 2019).

More recently, Bayerl and collaborators (2021) addressed the chromosomal abnormalities and loss of imprinting caused by culture in 5iLA, without compromising the expression of naive markers. Since mouse ESCs can tolerate the loss of epigenetic repressors, the group decided to screen for human naive conditions with the same property. They determined that inhibition of PKC, WNT, MEK and SRC was sufficient for induction of the naive state. The medium containing inhibitors for these pathways, as well as LIF, was denominated human enhanced naive stem cell medium (HENSM). Optional addition of Activin A, ROCK inhibitor and a P38/JNK

inhibitor were shown to boost the expression of naive markers (Table 1). Naive cells in this feeder-free condition present transcriptomic and epigenomic similarity to previously developed naive conditions, accumulate few chromosomal abnormalities upon extended culture and display pontual loss of imprinting. Using knockout cell lines, the authors also revealed differences between human and mouse naive pluripotency. While WNT signaling is important for mESCs, it must be inhibited for the establishment of human naive pluripotency. Additionally, *Klf17* is dispensable in mESC, but human *KLF17* knock-out cells differentiate and lose naive morphology (BAYERL et al., 2021). Figure 2 summarizes the main pathways and components associated with human naive pluripotency.

Figure 2: Diagram representing the main pathways and components associated with human naive pluripotency. Orange arrow represents a hypothesized interaction.

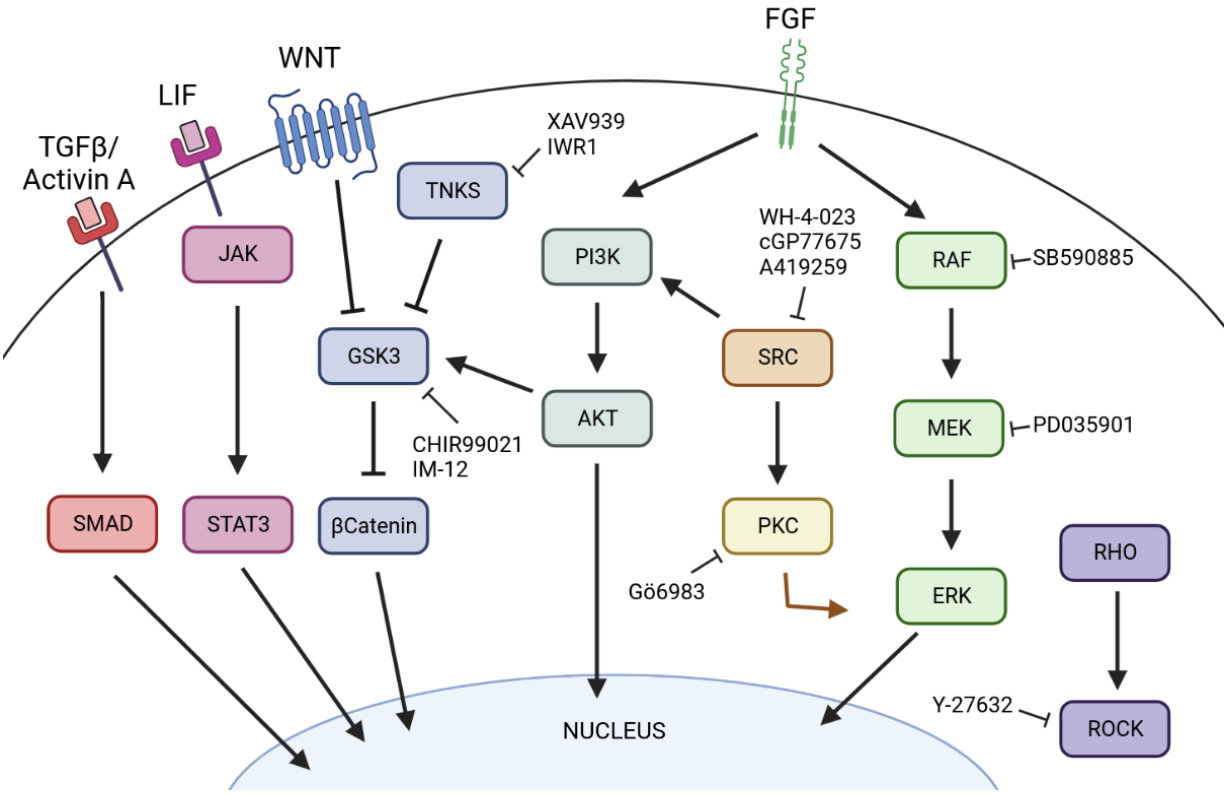

References: Adapted from Collier and Ruug-Gunn (2018).

Table 1: Composition of media for maintenance of hPSC. Xs and Os represent essential and optional components, respectively.

Reagent	Activity	t2iLGö	5iLA	PXGL	HENSM	LCDM	Expanded potential	4CL
LIF	JAK/STAT activator	X	X	X	X	X	X	X
Activin A	TGF-β/SMAD activator		X		O			X
PD0325901	MEK inhibitor	X	X	X	X			X
SB590885	B-RAF inhibitor		X				O	
WH-4-023	SRC inhibitor		X					
cGP77675	SRC inhibitor				X			
A419259	SRC inhibitor						X	
Gö6983	PKC inhibitor			X	X			
CHIR99021	GSK-3 inhibitor	X				X	X	
IM-12	GSK-3 inhibitor		X					
XAV939	Tankyrase inhibitor			X	X		O	
IWR1	Tankyrase inhibitor					O	O	X
Y-27632	Rock inhibitor		X		O	O		
DiM	Muscarinic M2 and histamine H1 receptors inhibitor					X		
MiH	PARP1 inhibitor					X		
Ascorbic acid	Demethylation						X	X
DZnep	Histone methyltransferase inhibitor							X
TSA	Histone deacetylase inhibitor							X

References: Takashima et al. (2014), Theunissen et al. (2014), Guo et al. (2017), Yang et al. (2017), Bredenkamp et al. (2019), Gao et al. (2019), Bayerl et al.(2021) and Mazid et al. (2022).

Many efforts have been made towards understanding the mechanisms and pathways modulated by the components of naive media. A 2019 study showed that the aPKC inhibitor Gö6983 and MEK inhibitor PD0325901 could be simultaneously replaced by a FGFR1 inhibitor in t2iLGö, suggesting that aPKC acts parallelly and downstream of MEK (LINNEBERG-AGERHOLM et al., 2019). Additionally, aPKC has been shown to be essential for nuclear localization of YAP and GATA3 expression in human embryos (GERRI et al., 2020). Accordingly, Gö6983 and tankyrase inhibitor XAV939 have been shown to reduce the levels of trophectoderm (TE) markers GATA3 and GATA2 in hPSCs (GUO et al., 2021). In particular, XAV939 prevents trophectoderm formation by limiting nuclear YAP (DATTANI et al., 2022). In the mouse, YAP nuclear localization via phosphorylation by LATS1/2, acquisition of cell polarity and trophectoderm differentiation depend on RHO–ROCK signaling (KONO; TAMASHIRO; ALARCON, 2014). This could suggest an additional role for ROCK inhibitor Y-27632 in naive media.

Recently, multiple groups have reported the existence of a different pluripotent-cell state, resembling the human 8-cell stage (MAZID et al., 2022; TAUBENSCHMID-STOWERS et al., 2022; YOSHIHARA et al., 2022; YU, X. et al., 2022). Even though small proportions of 8-cell-like-cells (8CLCs) can be found in naive cultures (MAZID et al., 2022; TAUBENSCHMID-STOWERS et al., 2022; YU, X. et al., 2022), no medium for stable establishment and maintenance of these cells has been developed to date. Instead, different strategies have been employed for enriching for and sorting 8CLCs in culture.

Mazid et al. (2022) developed media capable of increasing the proportion of 8CLCs from less than 2% in naive media to 11.9%. The 4 components and LIF (4CL) medium and its enhanced version (e4CL) include a histone methyltransferase inhibitor and a histone deacetylase inhibitor (Table 1). Taubenschmid-Stowers and collaborators (2022) found that *DUX4* overexpression could induce the transcription of genes typical of the EGA phase. They also suggest the use of *TPRX1* and *HY.3* as markers of the 8C-like state. In turn, Yoshihara et al. (2022) determined that transient expression of *DUX4* by a primed inducible cell line caused up to 17% of the cells to present transcriptional similarity to the early embryo. Additionally, they propose that the surface marker sodium-dependent phosphate transporter (NaPi2b) can be used to

sort for 8CLCs. Finally, X. Yu and collaborators (2022) found cells more similar to 8-cell stage blastomeres than naive through a chemical screening. The group developed a reporter line that employed the putative promoter of *LEUTX*, an EGA marker, for mCherry expression, and used it to find new culture conditions that could support 8CLCs.

1.4 - X chromosome inactivation in pluripotent stem cells

XCI is one of the fundamental properties used for the definition of pluripotency states. At the same time, PSCs can potentially be employed in the study of XCI. Throughout the years, multiple efforts have been made towards characterizing XCI in PSCs and understanding the relationship between them.

Eggan et al. (2000) investigated XCI in embryos cloned by nuclear transfer using transgenic mice with an X-linked GFP reporter. The authors verified that GFP was detected in E12.5 embryos regardless of parent of origin, but only maternally-inherited GFP was expressed in the placenta. In turn, upon transfer of mESCs nuclei, expression of both *Xist* alleles was detected in the placenta and the epiblast at E13.5. This suggested that the nuclei of mESCs do not keep imprinting-related epigenetic marks, allowing random XCI. Later, Maherali and collaborators (2007) determined that mouse iPSCs do not express *Xist* and present biallelic expression of *Tsix* and *Pgk1*, an X-linked gene. They proceed to show that, upon differentiation, mouse iPSCs carrying a monoallelic X-linked fluorescent reporter undergo random XCI, displaying one *Xist* and one *Tsix* focus per cell. All this evidence indicated that mESCs and mouse iPSCs could properly recapitulate embryonic XCI and could be used to dissect the mechanism *in vitro*.

Soon after, Navarro and collaborators (2008) showed that pluripotency factors NANOG, OCT3/4 and SOX2 bind *Xist* intron 1 in the mouse, suggesting a link between X chromosome reactivation (XCR) and pluripotency. While NANOG is not required for OCT3/4 and SOX2 binding, its depletion triggers moderate *Xist* upregulation (NAVARRO et al., 2008). In the following year, Donohoe et al. (2009) found that OCT4, but not SOX2, is essential for X-X chromosome pairing and counting in female mESCs. Subsequently, pluripotency-related factors REX1 and

PRDM14 have also been shown to bind *Xist* intron 1 and regulate XCI in the mouse (GONTAN et al., 2012; PAYER et al., 2013). However, in 2013, Minkovsky et al. generated *Xist* intron 1 mutant mouse models and showed that the region is not required for XCI and XCR. More recently, Janiszewski and collaborators (2019) assessed the timing of XCR during mouse iPSC reprogramming. They found that a group of genes, mainly located close to XCI-escaping genes, is reactivated before the induction of late pluripotency factors. Genes of this group displayed enrichment for sequences that bind pluripotency-related transcription factors, while genes whose reactivation is delayed were enriched in the YY1 motif, involved in the recruitment of *Xist*. They proposed that, although *Xist* intron 1 may help regulate XCI and XCR, the processes are probably also controlled by additional still undefined regions.

In contrast, the link between XCI and pluripotency in humans remains largely unexplored. Shen et al. (2008) showed that, unlike mESCs and mouse iPSCs, hESCs in the primed state present a single active X chromosome, regardless of *XIST* expression. The authors also revealed that loss of *XIST* in hESCs was accompanied by a decrease in methylation in around 12% of the X-linked CpG islands, suggesting reactivation of up to 51 genes spread across the chromosome. This primed *XIST*-negative XCI state, denominated X chromosome erosion, was associated with extended culture and could not be reversed upon differentiation (SHEN et al., 2008; SILVA et al., 2008). Further studies confirmed that the XCI state of human somatic cells is maintained upon reprogramming (MEKHOUBAD et al., 2012). Human iPSCs were also shown to be subject to X chromosome erosion, with promoter demethylation leading to biallelic expression of previously silenced genes across the chromosome (MEKHOUBAD et al., 2012; NAZOR et al., 2012).

In 2017, Sahakyan and collaborators used RNA-FISH and RNA sequencing to characterize the XCI status of cells in naive medium. The group found that, upon naive conversion, *XIST* was silenced for multiple passages. Even though *XIST* foci were detected in most cells after 19 passages in 5iLAF medium, the blastocyst stage-like biallelic *XIST* expression was recapitulated by only 5% of cells. Conversely, *XIST* expression was not detected in 97% of cells cultured in t2iLGö in passage 14, with the other 3% exhibiting monoallelic expression. The proportion of hESCS presenting biallelic *XIST* expression in early passages after derivation from the

preimplantation blastocyst, instead, reached 30%. Upon repriming, naive cells almost always re-inactivated the previously inactive allele and were unable to model random XCI. Still, naive conversion followed by repriming could reverse X chromosome erosion.

The authors also noticed a decrease in total expression of X-linked genes, but not autosomes, when cells transition from the *XIST* negative to positive states. This led them to suggest that cells would undergo X chromosome dampening (SAHAKYAN et al., 2017) (Figure 1B). However, more recently, new conclusions were drawn from a reinterpretation of the same dataset. Mandal and collaborators (2020) noticed that, even though the empirical cumulative distribution of expression of X-linked genes seemed to visually change between early and late clones, the total expression levels of X-linked genes was not significantly different between the two groups. At the same time, the group showed that the number of biallelically expressed SNPs was very variable between cells, but overall increased from early to late naive passages. To explain the data, they proposed that, instead of X chromosome dampening, *XIST*-negative cells presented incomplete X reactivation. Additionally, total expression of X linked genes could be explained by the upregulation of the active X in primed cells according to Ohno's hypothesis, returning to autosome-like levels after multiple passages (Figure 1B).

In the same year, An et al. (2020) used a fluorescent reporter line, containing different colored reporters inserted into each allele of the X-linked gene *MECP2*, to study the heterogeneity of cell states present in naive cultures. The authors showed that, while most cells cultured in 5iLA expressed both copies of the *MECP2* gene, a group displayed higher levels of tdTomato, the previously inactivated allele, as well as increased expression of naive pluripotency markers and higher proportion of biallelic *XIST*. The group found that these cells expressed high and low levels of FGF4 and FGF2, respectively, while the opposite trend was detected in the cells with lower tdTomato expression. Further tests, including addition of FGF2 in the culture medium and inhibition of FGF receptors, suggested that the heterogeneity was caused by incomplete blocking of FGF signaling. However, the authors also point out that total FGF inhibition was unsustainable due to high cell mortality. Surprisingly, high tdTomato cells were able to recapitulate random XCI upon repriming.

The main human and mouse PSC conditions, as well as their X chromosome states have been summarized in Table 2.

Table 2: Characteristics of stem cell-based models for the study of XCI *in vitro*

Organism	Model	Equivalent embryonic stage	XCI state	XIST expression	XCI upon differentiation
Mouse	mESc	Preimplantation epiblast	XaXa	Not expressed	Random
	mEpiSC	Postimplantation epiblast	XaXi	Monoallelic	-
Human	Naive hPSC	Preimplantation epiblast	XaXa	Not expressed/ Monoallelic/ Biallelic	Skewed/ Random
	Primed hPSC	Postimplantation epiblast	XaXi XaXe	Monoallelic (XaXi)/ Not expressed (XaXe)	-
	8CLCs	8 cell stage	?	?	?
	EPSC	Perimplantation epiblast	?	?	?
	Blastoids	Blastocyst	?	?	?

References: Evans and Kaufman (1981), Martin (1981), Thomson (1998), Eggan et al. (2000), Shen et al. (2008), Silva et al. (2008), Mekhoubad et al. (2012), Nazor et al. (2012), Theunissen et al. (2014), Sahakyan et al. (2017), Y. Yang. et al. (2017), Yu et al. (2021) and Mazid et al. (2022).

1.5 - Stem cell-based models of early development

Among the extensive applications of stem cells is their potential to model developmental processes *in vitro*. In 1998, the first trophoblast stem cell (TSC) line was derived from the murine blastocyst and extraembryonic ectoderm. The cell line is able to self-replicate while maintaining the capacity to differentiate into all subtypes of placental cells (TANAKA, 1998). In turn, a protocol for generation of human TSCs was only developed 20 years later. Cytotrophoblast (CT) cells are placental progenitors, capable of differentiating into extravillous cytotrophoblast and syncytiotrophoblast cells. When Okae et al. (2018) studied the transcriptome of

different placental cell types, they noticed that WNT and epidermal growth factor (EGF) pathways were overrepresented in CT cells. They used this information to develop a medium for *in vitro* maintenance of human TSCs composed of EGF and GSK3, TGF-β, histone deacetylase and ROCK inhibitors (OKAE et al., 2018).

A parallel strategy has been the derivation of human TSCs directly from PSCs. Initial reports claimed that TE-like cells could be induced by bone morphogenetic protein (BMP) (AMITA et al., 2013; YABE et al., 2016). Later, the extended pluripotency state was described by Yang et al. (2017) as an alternative to naive conditions, with greater differentiation potential. The LCDM chemical cocktail, including a muscarinic M2 and histamine H1 receptors inhibitor and a PARP1 inhibitor, was used to convert both mouse and human PSCs into the extended pluripotency stem cells (EPSC) (Table 1). While both mouse and human EPSCs were able to contribute to embryonic and extraembryonic tissues in mouse chimeras, mouse EPSCs could also give rise to whole mice by tetraploid complementation (YANG, Y. et al., 2017). The LCDM condition was later adapted for feeder-free culture of EPSCs (ZHENG et al., 2021).

Shortly after, extraembryonic contribution was also obtained with mouse cells in a new culture condition, denominated expanded potential (YANG, J. et al., 2017). In 2019, the medium was adapted for human and porcine cells. Besides contributing to embryonic and extraembryonic tissues in mouse chimeras, human cells in this state could be directly differentiated into TSCs (GAO et al., 2019) (Table 1).

More recently, Guo and collaborators (2021) were able to derive trophoblast stem cells directly from naive hPSCs cultured in PXGL. They showed that while MEK inhibition was sufficient for TSC induction, TGF-β inhibition could potentialize its effect. After only 5 days of culture, trophectoderm, cytotrophoblast and syncytiotrophoblast-like cells could be detected by scRNA-seq. Interestingly, conversion of primed hPSCs using the same strategy generated amnion-like cells. Re-analyzed transcriptomics data of TSCs derived from expanded potential stem cells (GAO et al., 2019) and through a BMP-based condition (YABE et al., 2016) displayed greater resemblance to amnion-like cells induced from primed PSCs than TSCs derived from PXGL cells. Finally, the authors showed that human early inner cell mass (ICM) cells, unlike mice, are able to differentiate into trophectoderm.

In 2018, Rivron and collaborators generated the first tridimensional model of the blastocyst stage composed solely of stem cells. The authors combined mESCs and TSCs in microwells, and showed that, within 3 days, the cells self-organized in blastocyst-like structures, denominated blastoids (RIVRON et al., 2018). More recently, two groups were able to culture synthetic mouse embryos up to E8.5 (AMADEI et al., 2022; TARAZI et al., 2022). Both strategies included the use of mESCs and induced extraembryonic endoderm stem cells generated by transient expression of *Gata4*. However, while the first used TSCs derived from extra-embryonic precursors, the second transiently induced *Cdx2* in mESCs to promote differentiation into TSCs. The aggregation step was carried out in AggreWell plates, and blastoids were later transferred to a roller culture system in both studies. Synthetic embryos recapitulated key organogenesis events, including the formation of a beating heart (AMADEI et al., 2022; TARAZI et al., 2022)

In 2021, two groups simultaneously developed the first protocols for generation of human blastoids (LIU et al., 2021; YU et al., 2021). One of the groups aggregated cells with transcriptional signatures close to epiblast, primitive endoderm and trophectoderm directly generated from reprogrammed dermal fibroblasts (LIU et al., 2021). However, it was later suggested that the trophoblast-like cells from this study more closely resembled the amniotic ectoderm (ZHAO et al., 2021).

On the other hand, Yu et al. aggregated naive PSCs in AggreWell plates for 8 or 9 days, sequentially employing hypoblast and trophoblast differentiation media (HDM and TDM, respectively). Blastoid cells presented correctly distributed epiblast, primitive endoderm and trophectoderm lineage markers, as confirmed by immunofluorescence and scRNA-seq. Some of the study's limitations include a great number of uncommitted cells and low protocol efficiency (YU et al., 2021). More recently, L. Yu and collaborators (2022) improved the TDM medium used in their protocol (Table 3) and showed that blastoids cultured on endometrial cells can model implantation.

Later in 2021, Yanagida and collaborators developed an alternative method for human blastoid generation. The group employed ultra-low attachment plates, followed by 96-well U-bottom plates, and blastoid formation was achieved within 3 days. For 2 days, blastoids were kept on the trophectoderm differentiation medium described by

Guo et al. (2021). Next, the MEK inhibitor was removed for the last 24 hours (Table 3). Characterization was performed by immunostaining and scRNA-seq of both blastoids and blastocysts.

Table 3: Composition of the main media for generation of human blastoids.

Reagent	Activity	L. Yu et al. (2022)		Yanagida et al. (2021)		Kagawa et al. (2022)	
		Days 0-3 (HDM)	Days 3-8 (TDM)	Days 0-2	Days 2-3	Days 0-2 (PALLY)	Days 2-4
FGF	FGF activator	X					
LIF	JAK/STAT activator		X			X	
Activin A	TGF-β/SMAD activator	X					
A83-01	TGF-β inhibitor		X	X	X	X	
PD0325901	MEK inhibitor		X	X		X	
SB590885	B-RAF inhibitor		X				
WH-4-023	SRC inhibitor		X				
CHIR99021	GSK-3 inhibitor	X					
Y-27632	Rock inhibitor					X	X
LPA	Hippo inhibitor		X			X	X

References: Yanagida et al. (2021), Kagawa et al. (2022) and L. Yu et al. (2022).

In the same year, two studies reported the generation of blastoids from EPSCs (FAN et al., 2021; SOZEN et al., 2021). However, concerns such as limited transcriptional similarity to human blastocysts, great proportion of undefined cells, medium composition including BMP4 and presence of amnion markers in

trophectoderm clusters were raised (LI; ZHONG; IZPISUA BELMONTE, 2022; LUIJKX et al., 2022).

Finally, in late 2021, Kagawa and collaborators published a new methodology for blastoid generation. The group's protocol was only 4 days long, reported an efficiency of over 70% and the characterized structures strongly resembled blastocysts, with very few unspecific or amnion-like cells (Table 3). Structures recapitulated embryonic milestones such as aggregation and sequential appearance of embryonic lineages. Blastoids were able to implant in 2D endometrial organoids, displaying expression of marker genes expected *in vivo*. Blastoid generation was originally performed in non-adherent hydrogel microwells made in-house, but the group has since adapted their protocol to commercially available plates, including 24-well AggreWell plates used in most other studies (HEIDARI KHOEI et al., 2023).

2 - Objectives

The process of XCI in human embryos has not been fully elucidated. The use of surplus embryos from *in vitro* fertilization in research poses significant problems, from low availability to genetic abnormalities.

In order to address these issues, the present work seeks to propose and evaluate alternative *in vitro* models for the study of XCI.

1. Evaluate the XCI state of pluripotent stem cells in previously unassessed conditions;
2. Analyze the process of XCI during blastoid formation.

3 - Materials and Methods

3.1 - Cell culture

The WIBR3 MECP2-GFP/tdTomato cell line was employed in all experiments (THEUNISSEN et al., 2016). The cell line is characterized by the presence of GFP and tdTomato endogenous reporters on each allele of the X-linked *MECP2* gene, which is subject to XCI.

Freezing vials were thawed at 37 ºC water bath for approximately 3 min. Cells were then transferred to 15 ml Falcon tubes with 1 ml FBS per vial and spun at 1000 rpm for 3 min. The medium was aspirated, cells were resuspended in the medium of choice. In order to improve cell survival, 50 nM Chroman 1, 5 µM Emricasan, and 0.7 µM Trans-ISRIB (CET cocktail) were added to the medium (CHEN et al., 2021) and plated in MEF or Geltrex coated 6-well plates at a density of 2.0×10^5 cells per well.

For passing, cells were washed with 2 ml PBS. Primed and naive cells were dissociated with Tryple Express and Accumax, respectively, for 3 min at 37 ºC. Cells were collected in 15 ml Falcon tubes and spun at 1000 rpm for 3 min. The medium was aspirated, cells were resuspended in the medium of choice containing the CET cocktail and counted on a Countess 3 automated cell counter. Cells were plated on MEF or Geltrex coated 6-well plates at a density of 2.0×10^5 cells per well. The CET cocktail was kept for 1 to 2 days, until cell-cell contact was established.

For freezing, cells were washed with 2 ml PBS and dissociated with Tryple Express for 3 min at 37 ºC. Cells were then collected and spun at 1000 rpm for 3 min. The medium was aspirated, cells were resuspended in the medium of choice containing the CET cocktail and counted. Cells were spun again and resuspended in the medium of choice containing the CET cocktail with 10% DMSO. Cells were divided across freezing vials totaling 500000 cells per tube.

Geltrex coated plates were prepared according to the manufacturer's instructions. For MEF coating, 6-well plates were coated with 2 ml of 0.1% gelatin for

at least 30 min. Meanwhile, frozen MEF vials were thawed in a water bath at 37 ºC for 3 minutes. Cells were then transferred to 15 ml Falcon tubes with 1 ml FBS and spun at 1000 rpm for 3 min. The medium was aspirated, and cells were resuspended in DMEM-F12. Excess gelatin in the 6-well plates was removed, and 2 ml of MEF-containing DMEM-F12 medium was added per well, so as to achieve a density of 1.5×10^5 cells per well.

3.2 - Naive state conversion and repriming

Upon passing, primed cells were resuspended on RESET medium (GUO et al., 2017) containing the CET cocktail and plated on MEF-coated plates at a density of 2.0×10^5 cells/well. After 3 days, the RESET medium was replaced with the naive medium of choice.

For repriming, cells were washed with 2 ml PBS, and the medium was replaced for the repriming medium of choice: mTSeR, N2B27 Basal supplemented with 2 μM XAV939 and FAC medium supplemented with 1 μM PD0325901. Repriming medium was changed every day for 3 to 5 days. Cells were then passed to Geltrex coated plates and medium was replaced with mTSeR.

3.3 - Media composition

For primed cell culture, mTSeR medium was used, and cells were cultured on Geltrex-coated plates.

PXGL naive medium (BREDENKAMP et al., 2019) is composed of 0.5% Knockout Replacement Serum, 1 μM PD0325901, 2 μM XAV939, 2 μM Gö6983 and 10 ng/ml LIF in N2B27 Basal medium. Cells were cultured on MEF-coated plates.

HENSM naive medium (BAYERL et al., 2021) is composed of 1 μM PD0325901, 2 μM XAV939, 2 μM Gö6983, 20 ng/ml LIF, 1.2 μM Y-27632, 1.2 μM cGP77675 and 50 μg/ml L-Ascorbic acid in N2B27 Basal medium. Cells were cultured on Geltrex-coated plates.

4CL medium (MAZID et al., 2022) is composed of 20 ng/ml LIF, 1 μM PD0325901, 20 ng/ml Activin A, 5 μM IWR1, 50 μg/ml L-Ascorbic acid, 10 nM DZNep, 5 nM TSA and 0.2% Geltrex in 4CL Basal medium. One liter of 4CL Basal medium in composed of 470 ml DMEM-F12, 470 ml Neurobasal medium, 10 ml non-essential amino acids, 10 ml Glutamax, 10 ml N2, 20 ml B27, 10 ml sodium pyruvate. Cells were cultured on MEF-coated plates.

LCDM medium (YANG et al., 2017) is composed of 10 ng/ml LIF, 2 μM Y-27632. 1 μM CHIR99021. 0.5 μM IWR-1. 2 μM (S)-(+)-Dimethindene maleate and 2 μM Minocycline Hydrochloride (MiH) in N2B27 Basal medium. Cells were cultured on MEF-coated plates.

RESET medium (GUO et al., 2017) is composed of 1 μM PD0325901, 10 ng/ml LIF and 1 mM valproic acid (VPA) in N2B27 Basal medium. Cells were cultured on MEF-coated plates.

Hypoblast Differentiation Medium (HDM) (YU et al., 2021), also known as FAC, is composed of 20 ng/ml ßFGF, 20 ng/ml Activin A and 3 μM CHIR99021 in N2B27 Basal medium.

Trophoblast Differentiation Medium (TDM) (YU, L. et al., 2022) is composed of 10ng/ml LIF, 1 μM PD0325901, 0.5 μM SB590885, 1 μm WH-4-023, 0.5 μM LPA and 1 μM A83-01 in TDM Basal medium. 50 ml of TDM Basal medium are composed of 36 ml DMEM-F12, 12 ml Neurobasal medium, 0.5% ITS-X, 250 μl non-essential amino acids, 250 μl Glutamax, 125 μl N2, 250 μl B27 and 0.1 mM 2-Mercaptoethanol.

One liter of N2B27 Basal medium in composed of 474 ml DMEM-F12, 474 ml Neurobasal medium, 10 ml non-essential amino acids, 10 ml Glutamax, 10 ml N2, 20 ml B27 and 0.1 mM 2-Mercaptoethanol.

3.4 - Flow cytometry

For collection, the medium was aspirated and cells were washed with 2 ml PBS. Cells were then dissociated with 1 ml Tryple Express for 3 min at 37 ºC. The medium was collected at 15 ml Falcon tubes, and cells were spun for 3 min at 1000

rpm. Medium was aspirated and cells were resuspended in 1 ml 4% PFA in PBS for fixation.

After 30 min, cells were spun again and the fixation medium was removed. Cells were then resuspended in 1 ml 4% BSA in PBS and transferred to cylindrical tubes for further analysis.

Calibur I and BD Biosciences LSR II were used for flow cytometry analysis, with a minimum of 10000 events. The software FlowJo was used for data analysis.

3.5 - RNA-FISH

RNA-FISH was performed according to the Biosearch Technologies Stellaris protocol. In the last passage before performing the experiment, cells were plated on 6-well plates containing a glass slip attached on Geltrex or gelatin before MEF plating, according to the cell matrix. When the desired confluence was obtained, cells were washed with 2 ml PBS and fixed with 4% PFA in PBS for 30 min. Cells were washed twice and permeabilized with 2 ml 70% ethanol per well for 1 hour to 1 week.

For hybridization, cells were washed with Wash Buffer A and incubated for 5 min. Meanwhile, to prevent evaporation of the probe. a humidified chamber was assembled by layering a water-saturated piece of paper towel and parafilm on a 6-well plate. The buffer was then aspirated from the cells and a 200 µl drop of the Hybridization Buffer was added to the parafilm on the humidified chamber. The coverslip was transferred cell-side down to the humidified chamber, and incubated in the dark at 37 ºC

After 4 to 16 hours, the coverslip was moved cell-side up to a new 6-well plate and incubated with 2 ml Wash Buffer A in the dark at 37 ºC for 30 min. Next, the buffer was aspirated and replaced with 2 ml of Wash Buffer A containing 5ng/ml DAPI. Again, cells were incubated in the dark at 37 ºC for 30 min. The buffer was then removed and cells were washed with 2 ml Wash Buffer B for 2 to 5 min. Finally, the coverslip was mounted onto a slide containing a 30 µl drop of Vectashield Mounting Medium. After the slides had dried completely, nail polish was added around the coverslip to prevent evaporation.

Wash Buffer A (10 ml) was composed of 2 ml Stellaris RNA-FISH Wash Buffer, 7 ml nuclease-free water and 1 ml deionized formamide. Hybridization Buffer (1 ml) was composed of 900 µl Stellaris RNA-FISH Hybridization Buffer, 100 µl deionized formamide. 1 µl of reconstituted Stellaris FISH Probes, Human *XIST* with Quasar 570 Dye was added to every 100 µl of Hybridization Buffer. Wash Buffer B had been previously prepared, by addition of 88 ml of nuclease-free water to the Wash Buffer B bottle provided by Stellaris.

3.6 - Variant Calling Pipeline

Single-cell RNA-seq data was generated by Wei Jiang's laboratory at the University of Wuhan. Feeder-free extended pluripotent stem cell data was obtained from web repository GEO, under accession code GSE137208, while unpublished embryonic stem cell data was sent directly to us.

Cutadapt was used to trim adapters and unremoved poly-A tails. Only transcripts at least 100 base pairs long were kept. FASTQ was used for quality control. Reads were aligned to the human reference genome assembly GRCh38 with HISAT2 version 2.2.1. Sambamba version 0.9.1 was used for SAM to BAM file conversion, sorting and filtering multi-mappers and duplicates. The data was then indexed with Samtools version 1.13.1 and HTSeq version 2.0.1 command *htseq-count* was used to quantify mapped reads.

Next, data was prepared for allele specific expression analysis. Reads not mapped to main chromosomes were removed with Samtools. In order to prepare data for the subsequent analysis, functions AddOrReplaceReadGroups, MarkDuplicates and SplitNCigarReads from Picard version 2.26.8 were employed: sample group information was included in BAM files, reads originated from the same RNA fragments were detected and marked and reads containing N in their CIGAR strings were split in order to account for alternative splicing.

For SNP calling, BAMs from all cells in the same condition were merged and the resulting file was sorted and indexed with Samtools. Next, GATK version 4.2.5.0 was employed in multiple operations. In order to detect sequencing errors and artifacts, base scores were recalibrated with functions BaseRecalibrator and

ApplyBQSR. Next, HaplotypeCaller was used for detection of SNPs. Due to the long running time of this operation, only chromosome X and controls 6, 7, 8 and 9, of similar size and number of genes, were analyzed. Heterozygous sites were detected and selected with SelectVariants.

Lastly, VariantFiltration was employed for quality control of the remaining SNPs. Argument "FS > 30.0" was used to filter out variants whose phred-scaled p-value of a Fisher's test to measure strand bias between reference and alternative allele reads is less than 30.0. Additionally, "QD < 2.0" filtered out variants with low quality when normalized by depth, in order to account for quality inflation in more highly covered regions. Once VCF files were ready, allele-specific counts for each cell were quantified with ASEReadCounter.

Data was subsequently analyzed with Python 3.8. Pandas package version 1.3.5 was used for data processing and plotting was done by Seaborn version 0.11.2 (BISONG, 2019). Statistical analysis was carried out with library Scipy.stats version 1.10.1 (VIRTANEN et al., 2020). Scripts employed in this work can be found at https://github.com/anaorsi/XCI-Analysis.

3.7 - Blastoid generation

Naive cells were dissociated with Tryple Express and resuspended in naive medium. For MEF removal, cells were plated on 0.1% gelatin-coated plates and incubated at 37 ºC for 15 min. The medium was gently collected and filtered in a 40 µm filter. Cells were then counted and spun at 1000 rpm for 3 min and resuspended in 1 ml FAC medium containing CET per well.

Aggrewell plates were coated with 500 µl of anti-adherence solution and spun at max speed for 5 min. Plates were incubated at room temperature for 15 min. Excess of anti-adherence solution was aspirated, and cells were plated at a density of 16 to 25 cells per microwell, or 19200 to 30000 cells per well. The plate was spun at 200 g for 1 min and carefully incubated in low O2 at 37 ºC.

After 2 days, if cells had grown quickly and the medium was yellow, an extra 1 ml of FAC medium was added to each well, in increments of 200 µl. On day 3, FAC medium was removed in 500 µl increments, wells were washed with 200 µl of PBS

and 1 ml of TDM medium containing CET was added in 200 µl increments. On the following days, an extra 1 ml of TDM medium was added to each well. After that, if necessary, the medium was partially changed by removal of 1 ml in 500 µl increments and addition of an extra 1 ml in 200 µl increments. Blastoids were generated by day 8 of the protocol.

3.8 - Blastoid immunofluorescence and imaging

Blastoids and earlier aggregates were collected at different timepoints, transferred to 40 µm cell strainers and fixed with 4% PFA in PBS. After 30 minutes, the structures were washed with 0.1% TX-100 in PBS for 5 minutes and permeabilized with 1% TX-100, 5% BSA in PBS for 30 minutes. After another wash, a 5% donkey serum, 0.1% TX-100 in PBS solution was used for blocking for 1 hour. Blastoids and aggregates were then washed one more time before staining with YAP primary antibody in donkey serum for one hour at 37 ºC or overnight at 4 ºC. Next, blastoids and aggregates were transferred from the primary antibody solution to a new solution containing the secondary antibody and 5 ng/ml DAPI. The plate was incubated in the dark for at least one hour. Finally, blastoids and aggregates were transferred to a 8-well Ibidi chambered coverslip. A Nikon CSU-W1 SoRa spinning disk confocal microscope was employed for imaging.

3.9 - Blastoid quantification

Blastoids were quantified using the software Imaris. For each day, four blastoids or aggregates were selected. Nuclei were identified and used for cell counting. Trophectoderm cells were characterized by YAP staining overlapping the nucleus only, while other cells were identified as components of the inner cell mass. Cells were further classified by overlapping GFP and tdTomato (TRITC) signals. Plotting and statistical testing was done via Python scripts, available at https://github.com/anaorsi/XCI-Analysis.

4 - Results

4.1 - Primed cell culture and characterization

The WIBR3 MECP2-GFP/tdTomato cell line was initially grown using a primed culture condition. Cells in mTSeR exhibited the expected morphology: flat colonies with smooth edges and poorly-defined cell boundaries (Figure 3A). RNA-FISH was conducted to check for *XIST* RNA distribution per cell. A single *XIST* cloud was observed in most cells (Figure 3B), as previously described in the literature (SAHAKYAN et al., 2017), indicating XCI.

Figure 3: Characterization of primed pluripotent stem cells. (A) Primed cell morphology in culture. (B) RNA-FISH of DAPI-stained primed cells for *XIST* RNA. (C) Flow cytometry of primed cells of the WIBR3 MECP2-GFP/tdTomato cell line for GFP and TRITC.

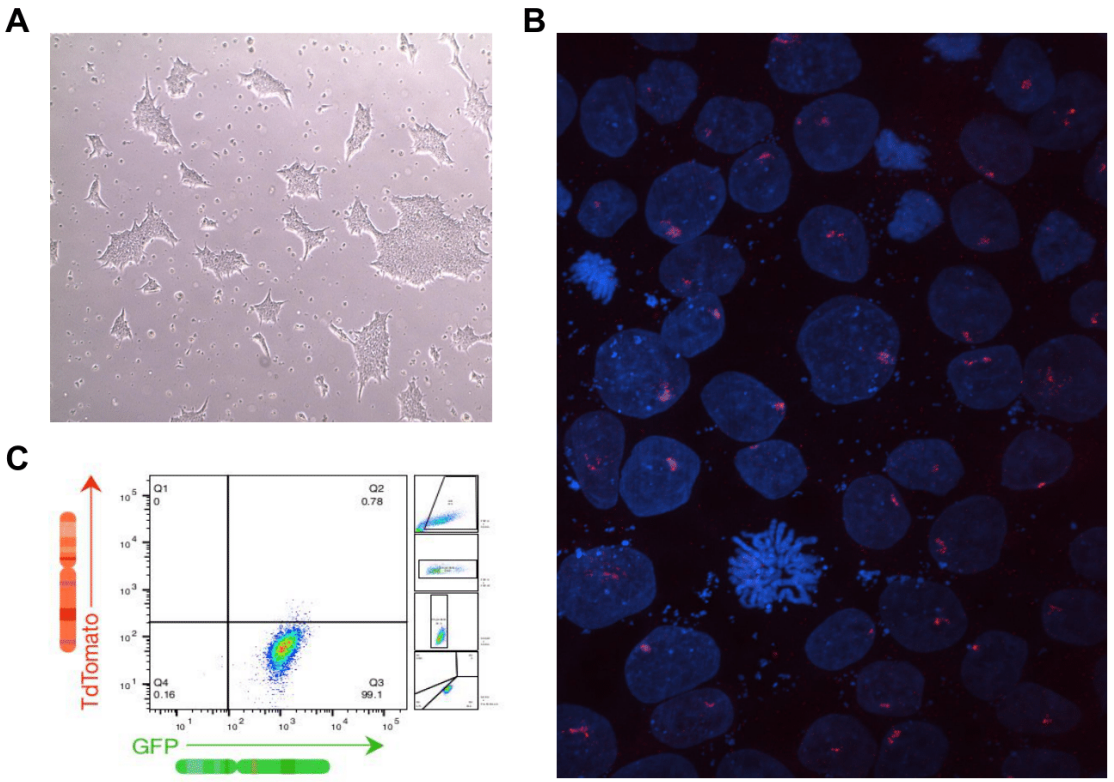

References: this work.

Next, we assessed the XCI status of the cells using the *MECP2* GFP and tdTomato reporters. Flow cytometry revealed a single cluster, composed of GFP-positive and tdTomato-negative cells (Figure 3C). This result indicated that cells presented a single active X chromosome. It also revealed that all cells had inactivated the same allele of the *MECP2* gene, which was expected, since the cell line used is clonal. The presence of a single *XIST* cloud and monoallelic expression of the *MECP2* gene suggest that cells cultured had not undergone X chromosome erosion.

Figure 4: Characterization of naive pluripotent stem cells in PXGL. (A) PXGL naive cell morphology in culture. (B) RNA-FISH of DAPI-stained naive cells for *XIST* RNA. (C) Flow cytometry of naive cells in PXGL along 3 passages (from left to right: 3, 8 and 13 days in total) of the WIBR3 MECP2-GFP/tdTomato cell line for GFP and TRITC.

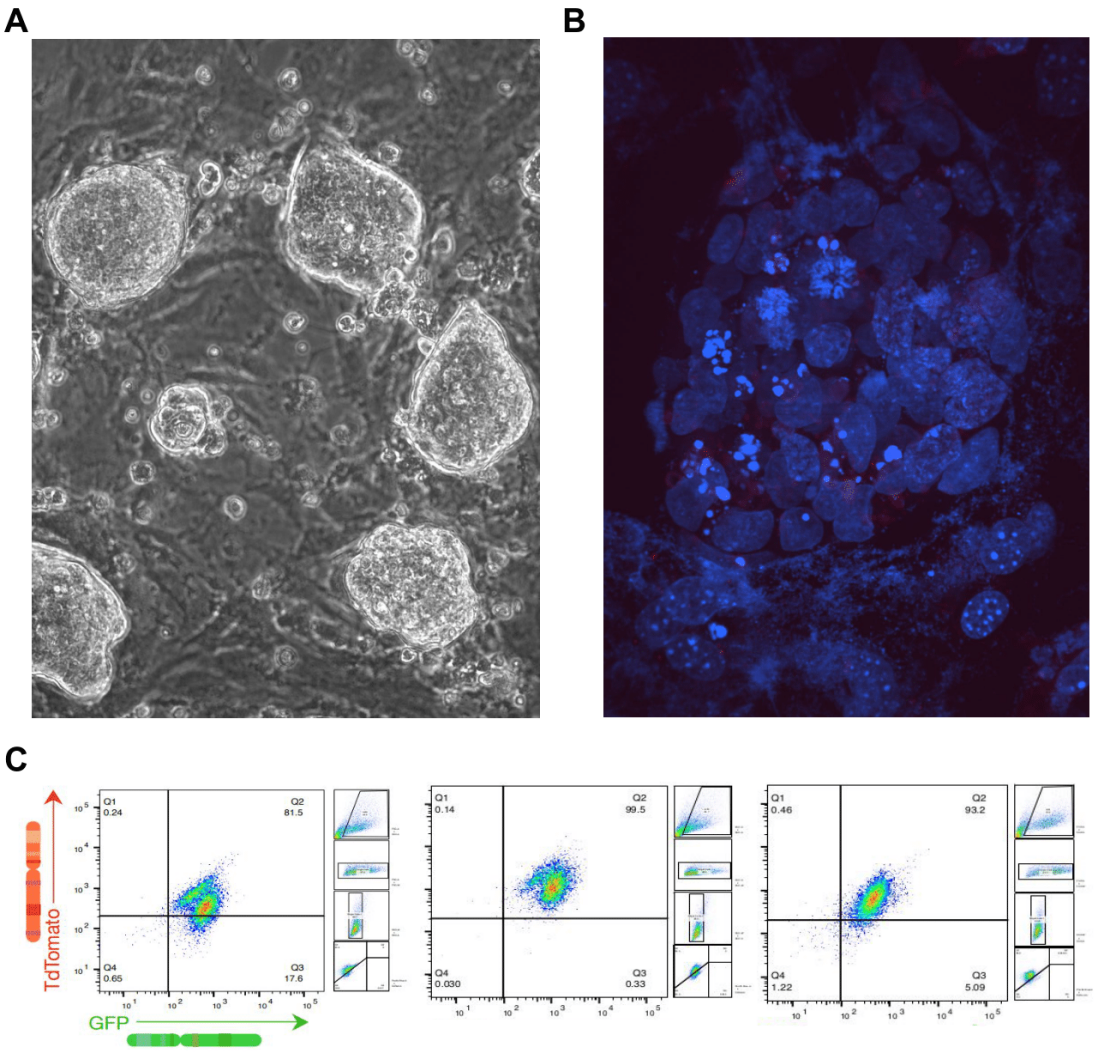

References: this work.

4.2 - Primed to naive conversion

After epigenetic resetting and a single passage in PXGL naive medium, small and bright dome-shaped colonies were observed (Figure 4A). *XIST* expression was not detected by RNA-FISH in PXGL cells in the second passage after naive conversion (Figure 4B). This result is consistent with previous studies showing that mono or biallelic expression of *XIST* is only induced after several passages (SAHAKYAN et al., 2017; AN et al., 2020).

Figure 5: Characterization of naive pluripotent stem cells in HENSM. (A) HENSM naive cell morphology in culture. (B) Flow cytometry of naive cells in HENSM along 2 passages (from left to right: 4 and 8 days in total) of the WIBR3 MECP2-GFP/tdTomato cell line for GFP and TRITC.

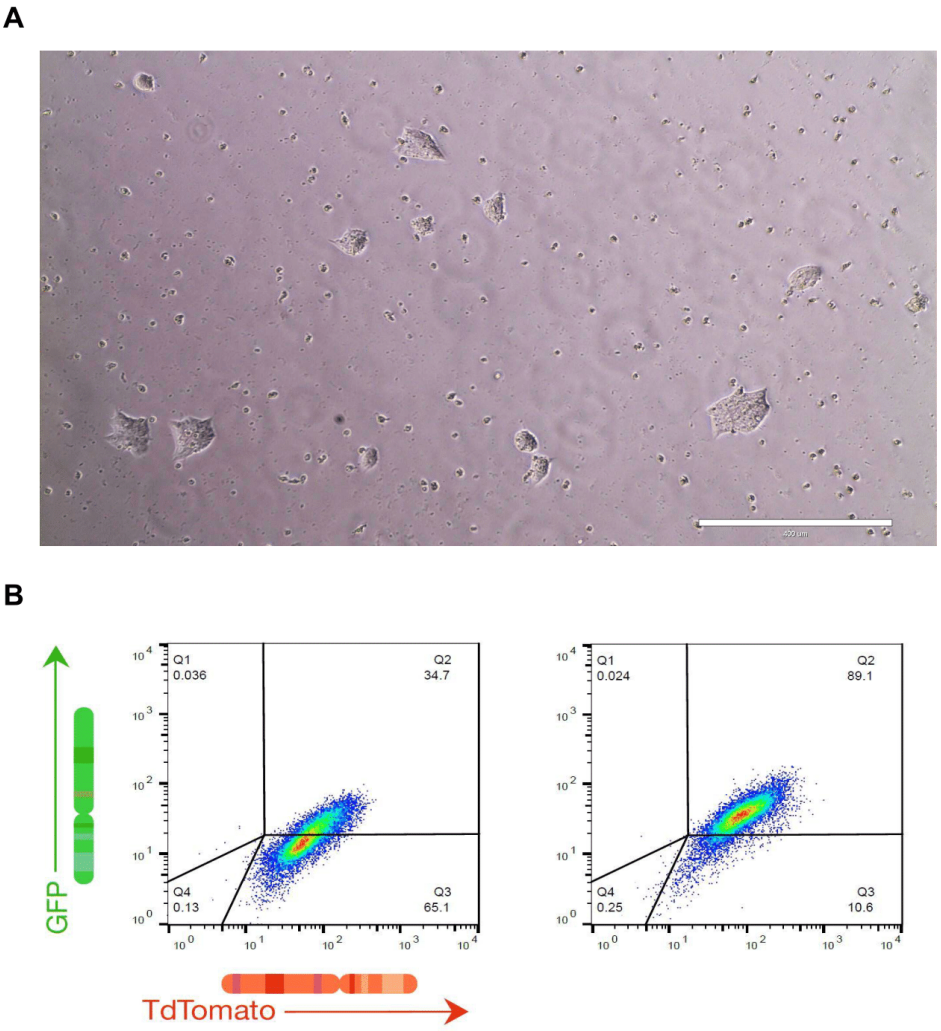

References: this work.

Flow cytometry analysis revealed that the majority of cells in this state were double-positive for tdTomato and GFP (Figure 4C). Similar results were observed in the two following passages, indicating that X reactivation of the previously inactive *MECP2* allele was maintained. Interestingly, from the first passage, cells seemed to be divided into two distinct double-positive subpopulations, expressing higher or lower levels of tdTomato. This segregation was still observed in passage 2, but was not perceptible in passage 3.

Next, XCR during primed to naive conversion using the HENSM condition was assessed. Cells were organized in small, bright and compact colonies (Figure 5A). Once again, reactivation of the previously inactive *MECP2* allele was observed from the first passage and sustained (Figure 5B). However, heterogeneity of tdTomato levels was not detected, and all cells formed a single cluster.

4.3 - XCI status of EPSCs

With the capacity to contribute to both embryonic and extra-embryonic tissues, EPSCs emerged as promising models for the study of early embryogenesis (YANG, Y. et al., 2017). However, to our knowledge, the XCI state of human EPSCs had not been previously assessed. We proceeded to determine whether EPSCs could be employed as *in vitro* models for XCI.

The X chromosome inactivation state of EPSCs was initially accessed *in silico.* Zheng and collaborators (2021) had previously used scRNA-seq to characterize cells of the H9 cell line cultured in feeder-free-EPSC and conventional primed conditions. The dataset was downloaded from the online repository GEO and the proportion of biallelically-expressed genes per chromosome was accessed for both EPSCs and primed ESCs, used as experimental control (Figure 6A). When compared to the analyzed autosomes, the X chromosomes of EPSCs displayed a significantly lower proportion of biallelically expressed genes. At the same time, there were no significant differences between biallelic expression proportions of the X chromosomes of EPSCs and ESCs. This suggested that, similarly to hESCs, EPSCs presented a single active X chromosome.

Figure 6: Evaluation of the XCI status of EPSCs. (A) Violin plots of the proportion of biallelically expressed genes linked to chromosomes X, 6, 7, 8 and 9 in EPSCs and primed ESCs. (B) EPSC morphology in culture. (C) Flow cytometry of the WIBR3 MECP2-GFP/tdTomato cell line EPSCs in LCDM medium for GFP and TRITC (two independent tests).

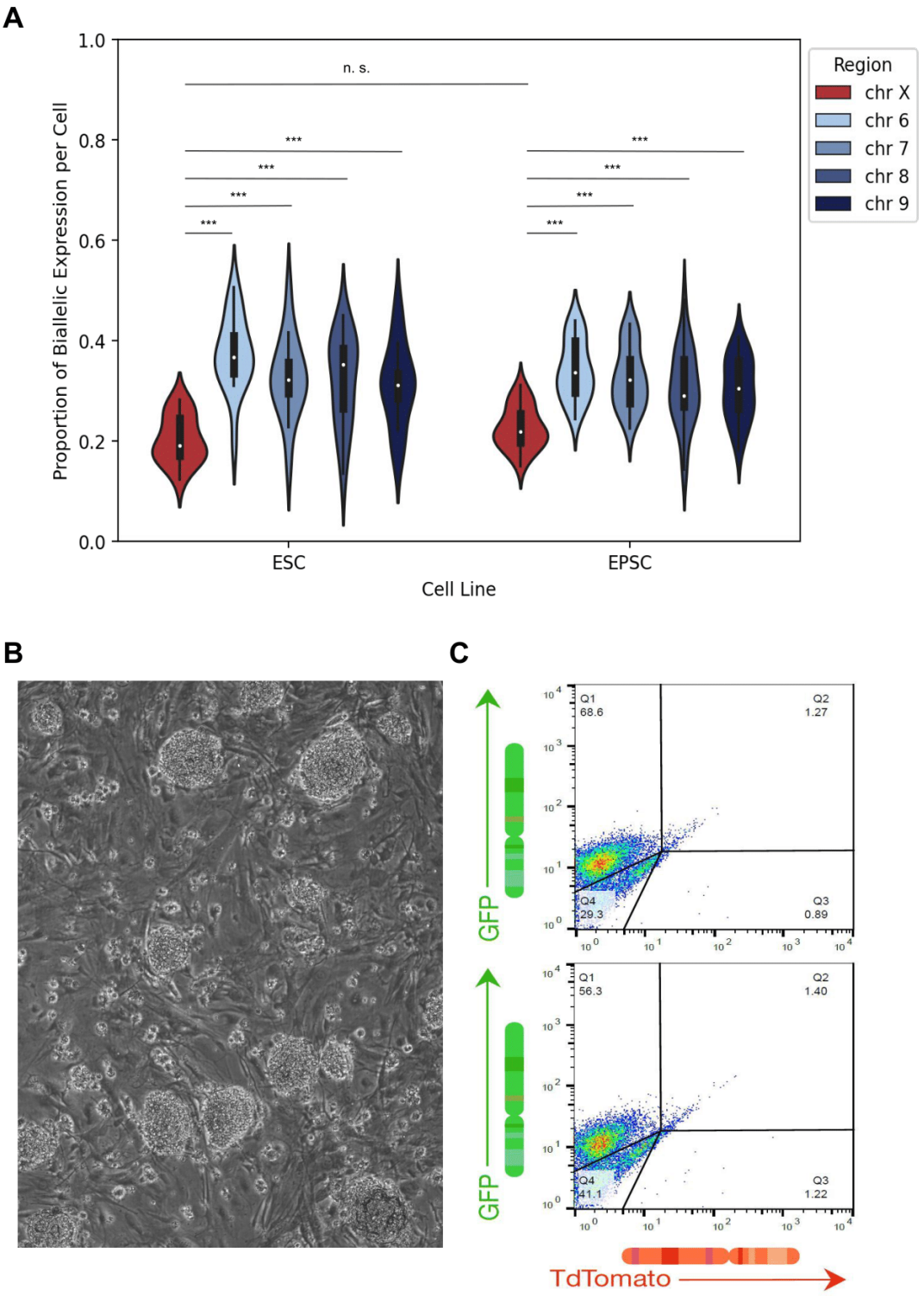

References: this work.

In order to test this hypothesis, cells from the WIBR3 MECP2-GFP/tdTomato line were cultured in LCDM medium for two passages. Upon EPSC conversion, cells formed large, well-defined and round colonies (Figure 6B). Flow cytometry analysis detected a majority of GFP positive/tdTomato negative cells in both passages analyzed, as well as a minority of cells co-expressing both markers (Figure 6C). These results corroborate the hypothesis that EPSCs have already undergone XCI and, therefore, are not suitable for the study of human XCI *in vitro*.

Figure 7: Evaluation of the XCI status of cells in 4CL medium. (A) Morphology of cells cultured in 4CL medium. (B) Flow cytometry of the WIBR3 MECP2-GFP/tdTomato cell line in 4CL medium for GFP and TRITC (two independent tests).

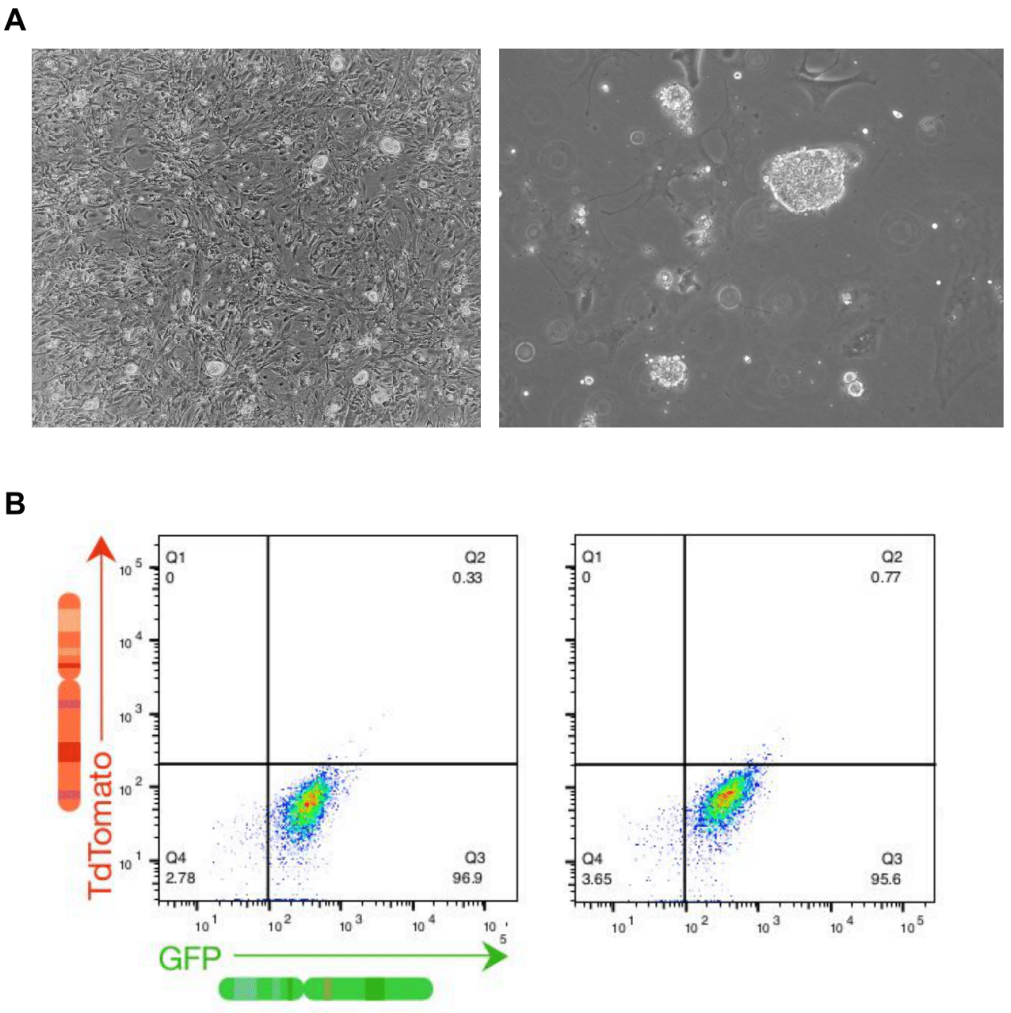

References: this work.

4.4 - XCI status of cells in the 4CL condition

Human 8-cell-like cells (8CLCs) were recently described as presenting close resemblance to blastomeres of the 8-cell stage (MAZID et al., 2022; TAUBENSCHMID-STOWERS et al., 2022; YOSHIHARA et al., 2022; YU, X. et al., 2022). However, previous studies did not assess the XCI state of cells in this condition. In one publication, authors described a naive medium with the capacity to increase the proportion of 8CLCs in culture, denominated 4CL (MAZID et al., 2022). Due to the similarity of 8CLCs to early stages of human development, this condition was tested as a candidate model for the study of XCI.

Primed cells were passed to MEF coated plates and the medium was changed to 4CL. After three days in culture, shiny round colonies could be detected (Figure 7A). However, flow cytometry analysis revealed that over 95% of cells presented a single active *MECP2* allele, even after 3 passages. In both attempts, less than 1% of the cells presented biallelic *MECP2* expression, less than the expected proportion of 8CLCs in the medium (Figure 7B). Therefore, due to the lack of X-chromosome inactivation, the 4CL medium does not satisfy the requirements defining naive pluripotency.

4.5 - XCI status upon repriming

Next, the capacity of naive cells to undergo XCI after repriming was tested. Three different media were employed for the re-priming of naive cells cultured in the 5iLA condition: mTSeR, N2B27 basal medium supplemented with XAV939, and FAC medium supplemented with PD0325901. Allelic specific expression of the *MECP2* gene was assessed by flow cytometry.

In all tests conducted, inactivation of the previously inactive Tomato-red-tagged allele was observed (Figure 8), indicating that, despite reactivation of the Xi, epigenetic marks of inactivation were maintained in that chromosome in naive cells. Therefore, random XCI could not be reproduced by repriming 5iLA cells.

Figure 8: Re-priming of naive cells in 5iLA medium. From left to right: FAC + PD0325901 medium, passage 1, N2B27 basal + XAV939 medium, passage 1 and FAC + PD0325901 medium, passage 4.

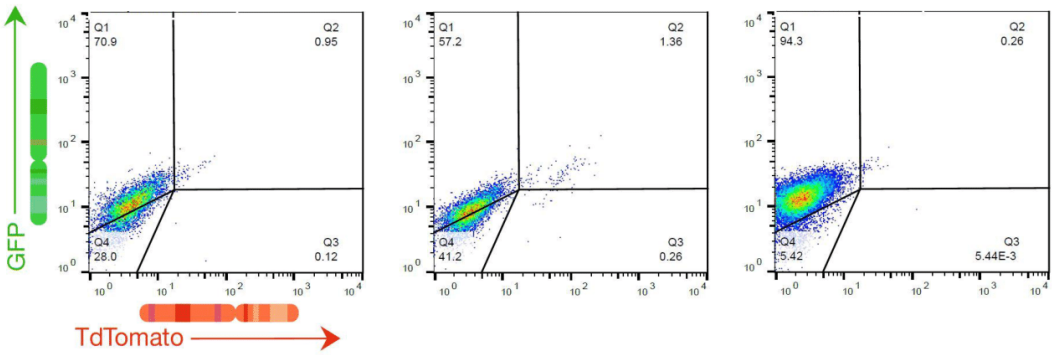

References: this work.

4.6 - XCI in blastoids

We then assessed XCI during blastoid formation, employing the WIBR3 MECP2-GFP/tdTomato hESC line converted into the naive state with PXGL medium. Blastoids were generated according to a recently updated protocol (YU, L. et al., 2022) and developed as expected. During the first 3 days, structures underwent compaction, characterized by loss of clear cell boundaries and round blastomere appearance. Next, at days 5 and 6, trophoblast-like cells, located in the edges of the structure and displaying flat morphology, were observed. On days 6 and 7, cavities could be detected. Structures progressively grew until the end of the protocol.

Figure 9: Day by day representative pictures of the blastoid generation process.

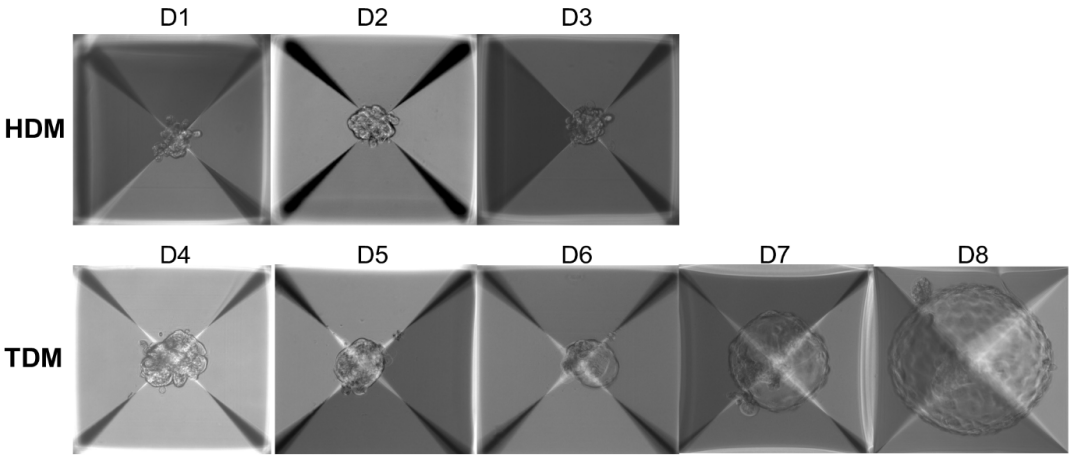

References: this work.

Aggregates were fixed and stained for YAP1 at the protocol days 1, 5 and 8. On the first day of the protocol, only low levels of cytoplasmic YAP1 could be detected. By day 8, both trophoblast-like cells, characterized by nuclear YAP1, and ICM-like cells, displaying cytoplasmic YAP1, were present and distributed as expected in the blastocyst-like structures (Figures 10 and 11).

Figure 10: Immunofluorescence images of blastoids generated with the MECP2-GFP/tdTomato cell line, stained for YAP1 and nuclear stained by DAPI, fixed at days 1, 5 and 8, first replicate.

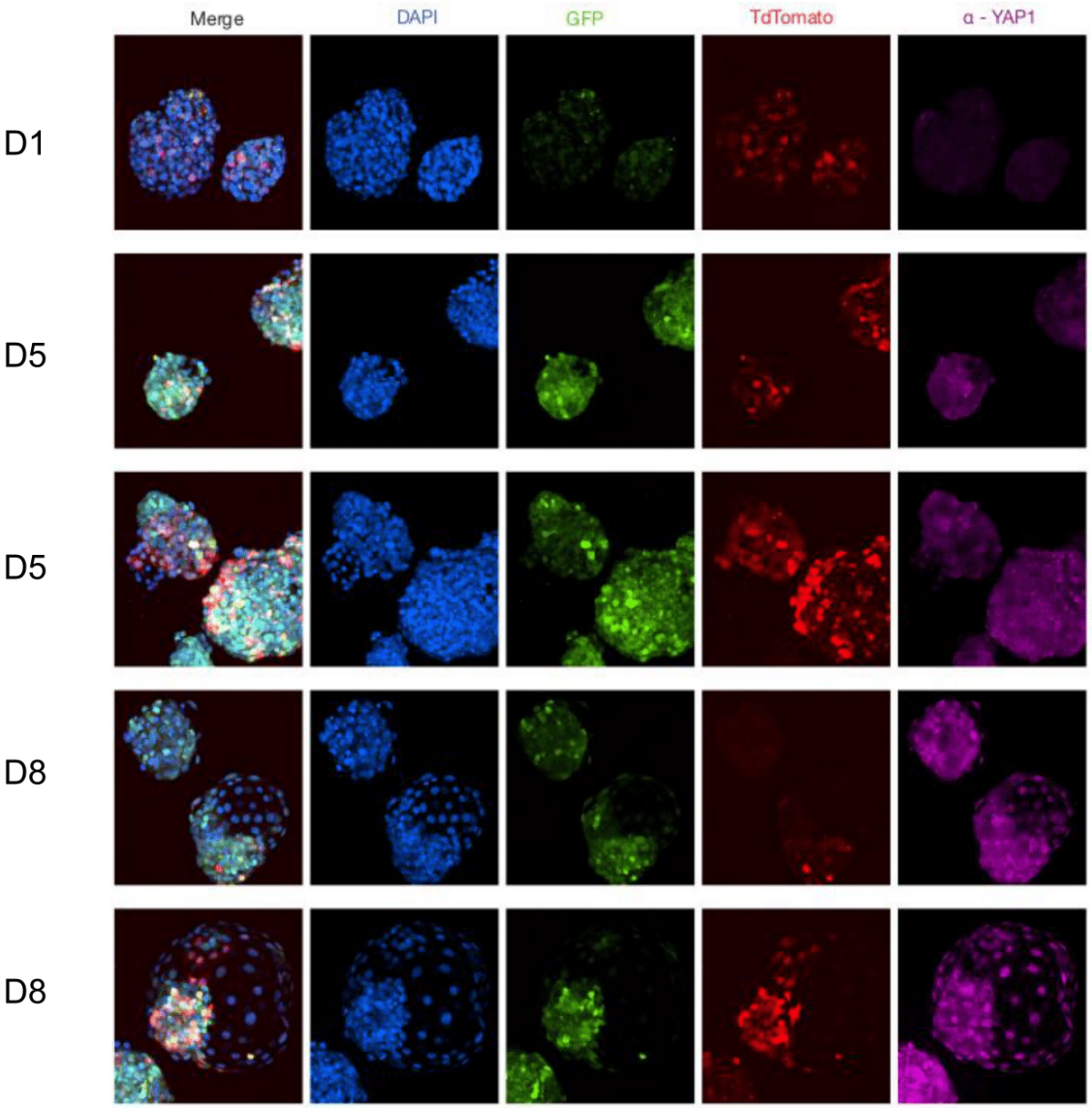

References: this work.

Figure 11: Immunofluorescence images of blastoids generated with the MECP2-GFP/tdTomato cell line, stained for YAP1 and nuclear stained by DAPI, fixed at days 1, 5 and 8, second replicate.

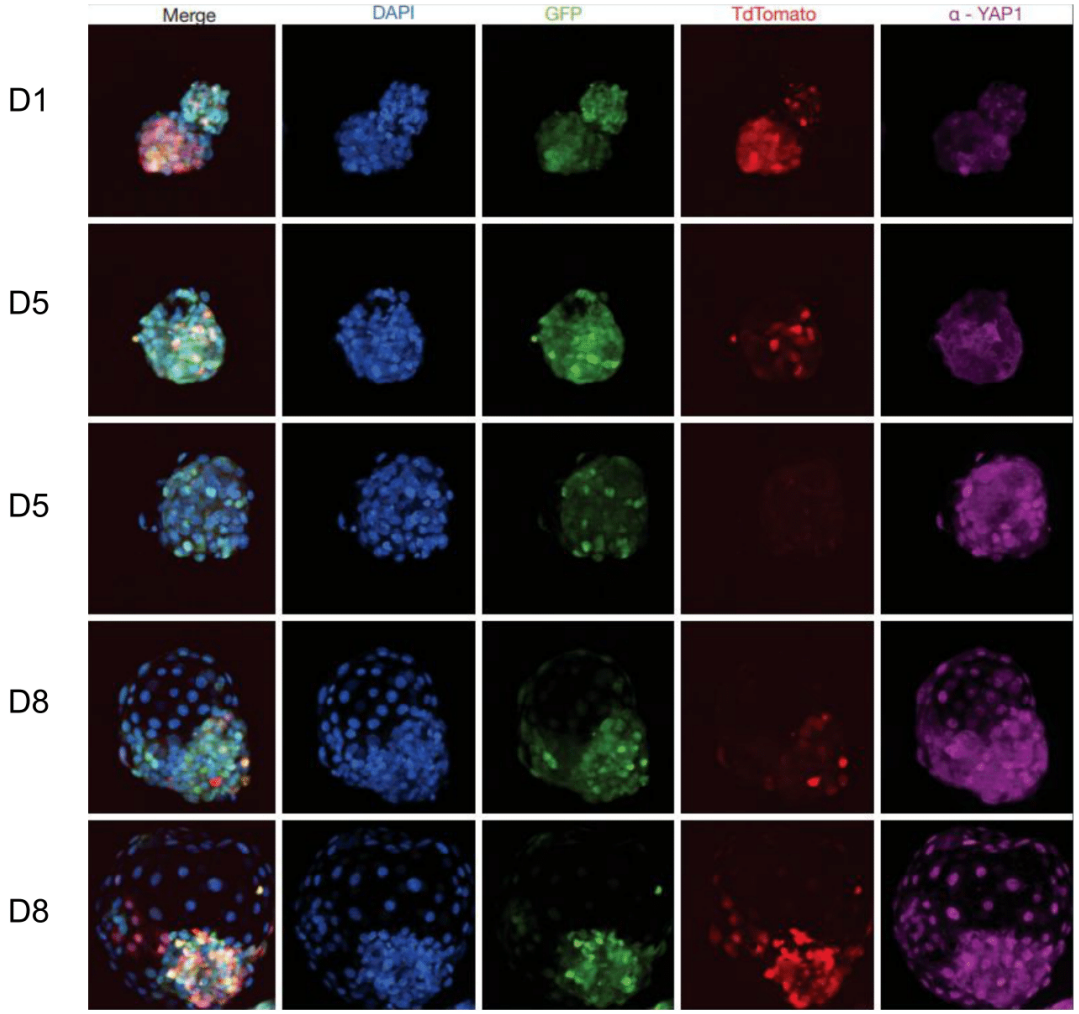

References: this work.

Immunofluorescence revealed progressive decrease in GFP and tdTomato coexpression, indicating inactivation of a single *MECP2* allele per cell (Figures 12A and B). Loss of biallelic expression was accompanied by increased intensity of the remaining allele (Figures 10 and 11). Overall, a significant bias towards re-inactivation of the previously inactive *MECP2* allele (tdTomato) was observed: out of all cells displaying monoallelic MECP2 expression, an average of 70% expressed GFP in all days assessed. (Figures 12B and C). A Wilcoxon signed rank test suggested that the observed ratio of GFP expressing cells was significantly higher than the expected unbiased median (0.5), with a p-value of 0.001.

Figure 12: XCI during blastoid generation. (A) Line plot representing the percentage of cells displaying mono or biallelic expression of MECP2 by protocol day. (B) Bar plot of the percentage of double positive, GFP+/tdTomato- and GFP-/tdTomato+ cells by protocol day. (C) Box plot showing the proportion of GFP+/tdTomato- cells out of all cells displaying monoallelic expression, with dashed line representing the hypothesized unbiased median.

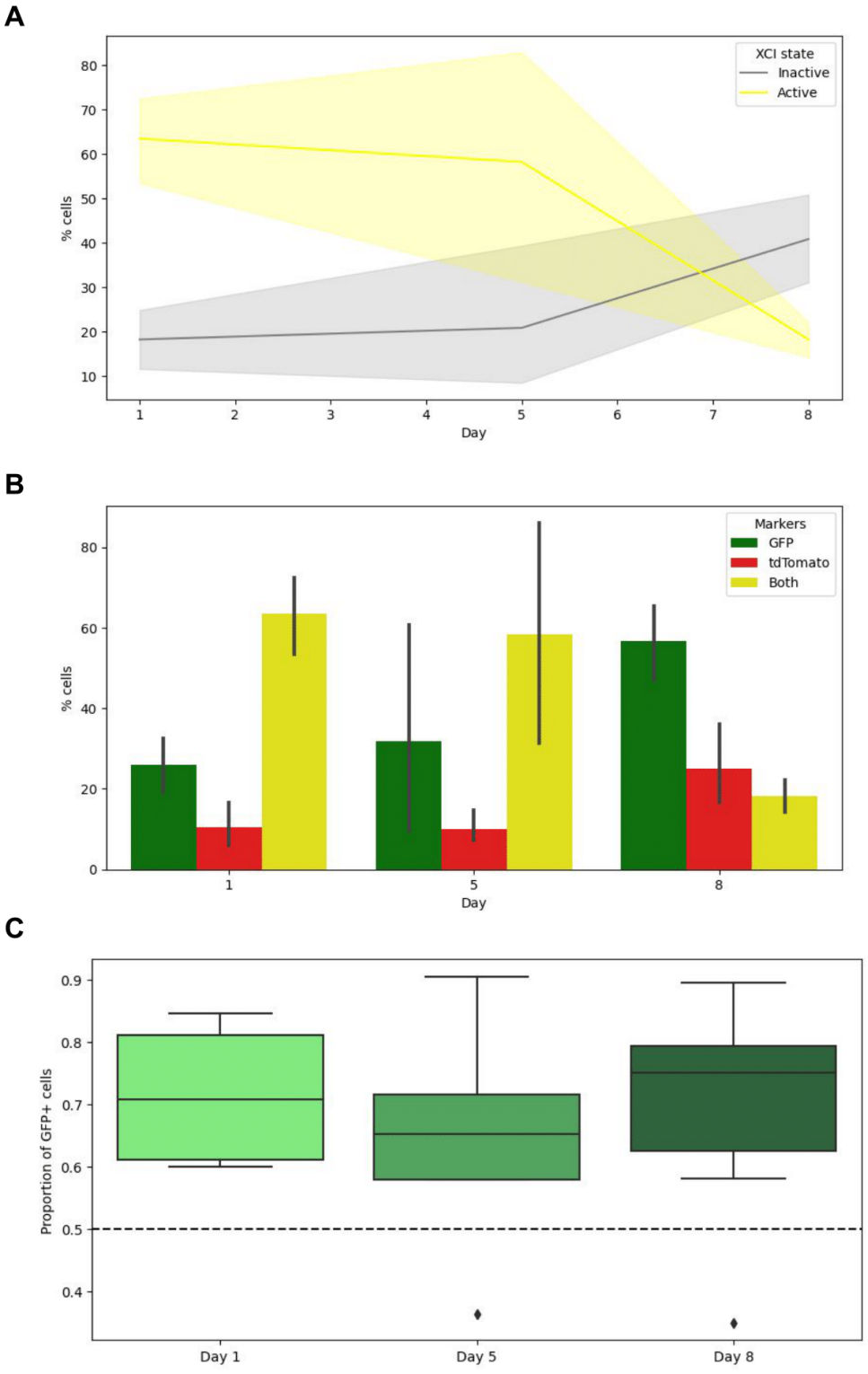

References: this work.

Figure 13: XCI comparison between trophoblast and ICM-like lineages. (A) Day 7 blastoid, displaying monoallelic expression of the *MECP2*-tdTomato allele in both ICM-like and trophoblast-like cells. (B) Bar plot representing the quantification of mono and biallelic *MECP2* expression by lineage in day 8 blastoids. (C) Bar plot representing the quantification of exclusive *MECP2*-GFP and *MECP2*-tdTomato expression by lineage in day 8 blastoids.

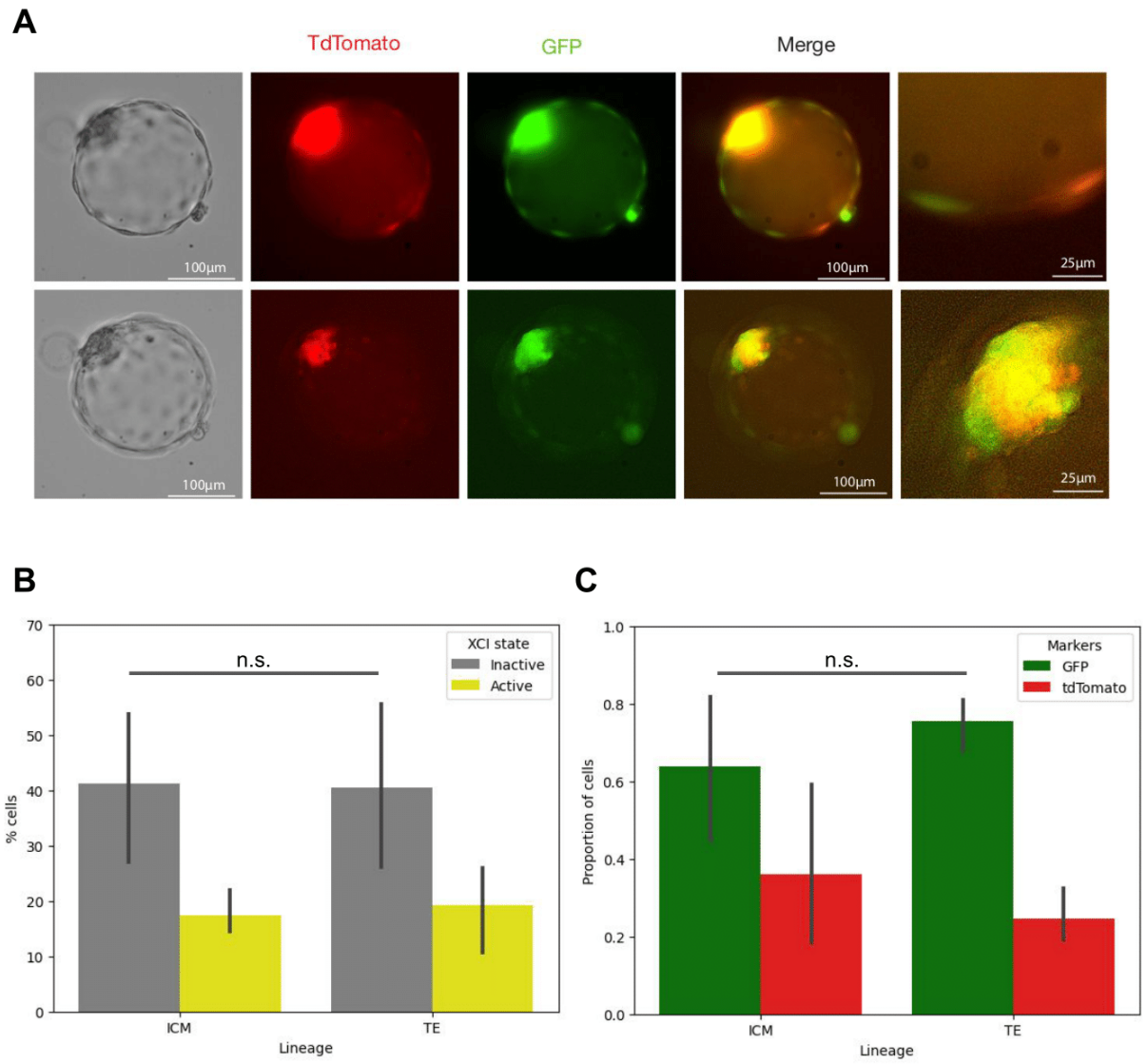

References: this work.

By the end of the protocol, both GFP+/tdTomato- and GFP-/tdTomato+ cells could be found in the inner cell mass and the trophectoderm (Figure 13A). This suggests that blastoids are capable of random XCI. Additionally, despite the increase of cells presenting monoallelic expression of *MECP2*, about 20% of the cells detected at day 8 still presented co-expression of GFP and tdTomato (Figures 12A, 12B and 13B). This indicates that XCI was not complete by the end of the protocol.

Finally, we assessed possible differences between the trophoblast and ICM-like lineages using Mann–Whitney U tests. The proportion of cells still displaying biallelic *MECP2* expression at day 8 was approximately the same for the two lineages (Figure 13B). Both trophoblast and ICM-like displayed a bias for inactivation of the tdTomato *MECP2* allele, but no statistically significant differences between the two samples were detected (Figure 13C).

Table 4 summarizes the main XCI-related properties of stem-cell based models, including the findings of this work.

Table 4: Updated characteristics of stem cell-based models for the study of XCI *in vitro*

Organism	**Model**	**Equivalent embryonic stage**	**XCI state**	**XIST expression**	**XCI upon differentiation**
Mouse	mESc	Preimplantation epiblast	XaXa	Not expressed	Random
	mEpiSC	Postimplantation epiblast	XaXi	Monoallelic	-
Human	Naive hPSC	Preimplantation epiblast	XaXa	Not expressed/ Monoallelic/ Biallelic	Skewed/ Random
	Primed hPSC	Postimplantation epiblast	XaXi XaXe	Monoallelic (XaXi)/ Not expressed (XaXe)	-
	8CLCs	8 cell stage	XaXi	?	-
	EPSC	Perimplantation epiblast	XaXi	?	-
	Blastoids	Blastocyst	XaXi XaXa	?	Skewed/ Random

References: Evans and Kaufman (1981), Martin (1981), Thomson (1998), Eggan et al. (2000), Shen et al. (2008), Silva et al. (2008), Mekhoubad et al. (2012), Nazor et al. (2012), Theunissen et al. (2014), Sahakyan et al. (2017), Y. Yang. et al. (2017), Yu et al. (2021), Mazid et al. (2022) and this work.

5 - Discussion

Here, different models for the study of human XCI *in vitro* were proposed and assessed. Initially, we characterized primed and naive cells cultured in various media. In all naive conditions, reactivation of the previously inactive *MECP2* allele was observed after very few passages. Further studies, assessing allelic-specific expression of more genes, will be necessary to test whether XCR is complete by this time point.

We also observed a single *XIST* focus in most primed cells cultured in mTeSR, which suggests that the cell line used had undergone XCI but not X chromosome erosion. In turn, upon naive conversion, cells cultured in PXGL did not present *XIST* expression during the first two passages. This is consistent with a previous report showing that naive cells go through a *XIST* negative state during the initial passages after naive conversion (SAHAKYAN et al., 2017).

The relationship between the signaling pathways regulating pluripotency and XCI remains unclear. Primed pluripotency depends on FGF/MEK/ERK, WNT and TGF-β signaling. In turn, human naive pluripotency is characterized by inhibition of FGF/MEK/ERK, WNT, SRC and aPKC. Surprisingly, while proliferation of mouse ESCs also requires inhibition of FGF/MEK/ERK, the WNT pathway must be activated in this model (THEUNISSEN et al, 2016; BAYERL et al., 2021). Since naive cells of both species present two active X chromosomes and undergo XCI upon repriming, the FGF/MEK/ERK seems the ideal candidate to link XCI and pluripotency states.

Previously, the FGF/MEK/ERK pathway has been associated with naive pluripotency and X chromosome activation in female cells. Genolet et al. (2021) sought to understand sex specific differences present during early development and mESC differentiation. Through a CRISPR screening, the group found two X-linked genes associated with naive pluripotency, *Dusp9* and *Klhl13*. DUSP9 dephosphorylates ERK and cells carrying two copies of the gene displayed decreased DNA methylation. In turn, disruption of a single copy of *Klhl13* led to increased levels of MAPK pathways target genes and a decrease in pluripotency genes. Additionally, An and collaborators (2020) have shown that incomplete blocking of

FGF2 signaling leads to heterogeneity of marker expression and XCI states in human naive cells. Further studies will be necessary to clarify the driving mechanisms of XCI and XCR in mouse and human PSCs.

Displaying high plasticity and unprecedented differentiation potential, EPSCs emerged as promising candidates for modeling human preimplantation development. Yet, recent works have been challenging this initial proposition. Guo and collaborators showed that TSCs derived from cells in LCDM medium present greater similarity to the amnion (GUO et al., 2021). In addition, our work provides computational and experimental evidence that female EPSCs have undergone XCI. These results suggest that EPSCs actually reflect a later embryonic stage and are not ideal for the study of early development.

One important limitation of EPSCs is their heterogeneity and poor characterization. The LCDM medium features CHIR99021, a GSK3 inhibitor and WNT pathway agonist, and does not contain any small molecules known to regulate the FGF/MEK/ERK pathway. Since WNT and FGF/MEK/ERK inhibition have been described as requirements for human naive pluripotency (BAYERL et al., 2021), EPSCs must represent a distinct pluripotency state, probably closer to primed cells. Additionally, components DiM, a muscarinic M2 and histamine H1 receptors inhibitor, and MiH, a PARP1 inhibitor, were discovered in a chemical screening. Previously, PARP1 deficiency in mPSCs has been shown to induce TE differentiation (HEMBERGER et al., 2003). Still, the precise role of each component in the regulation of extended pluripotency remains elusive. In the future, mechanistic studies may help us to better characterize the pathways modulated in EPSCs.

In this work, we assessed the XCI status of cells cultured in 4CL medium. It was previously suggested that this condition resembles the naive pluripotency state (MAZID et al., 2022). Our results suggest that, in terms of XCI, the medium does not satisfy the requisites to be considered naive. Because the 4CL medium is said to increase the proportion of 8CLCs in culture, we expected to find a separate cluster of cells in the flow cytometry data, displaying coexpression of tdTomato and GFP. Interestingly, this second group of cells could not be detected, suggesting that 8CLCs, if present, do not present 2 active X chromosomes. It could be argued that the 8CLCs were not numerous enough to be clearly distinguished by flow cytometry essay.

Yoshihara and collaborators (2022) suggested that surface marker NaPi2b is 8CLC-specific and can be used for sorting. It would be interesting to employ this technique to analyze the XCI status of 8CLCs in particular and test the hypothesis presented.

Sahakyan and collaborators (2017) previously showed that, upon repriming, naive hPSCs cultured in 5iLAF do not undergo random XCI, and instead tend to inactivate the previously silenced X chromosome. Here, we obtained similar results upon repriming of cells cultured in 5iLA medium. These observations suggest that, even though PSCs undergo XCR upon naive conversion, an epigenetic memory of XCI must exist, leading to inactivation of the previously inactive allele and preventing random XCI in most cases. Female hESCs and hiPSCs, derived from the epiblast and somatic tissues, respectively, have already undergone one round of XCI and will likely carry an epigenetic memory, preventing *in vitro* modeling of random XCI. One way to overcome this issue would be to derive PSCs from an earlier cell population in the embryo, prior to the first round of XCI. Morula cells, presenting more blastomeres than earlier stages and available in fertility clinics, would be the ideal candidates for this experiment.

In 2020, An et al. revealed the presence of two cell subpopulations in the same culture condition by flow cytometry. One of the groups, characterized by higher levels of naive markers and greater proportions of cells with biallelic *XIST* expression, could undergo random XCI upon differentiation. In this study, we observed similar results with cells cultured in PXGL: two clusters were detected by flow cytometry and blastoids generated by these cells could undergo random XCI. Still, skewness for inactivation of the previously active allele was observed. Further studies will be necessary to determine ways to reduce the heterogeneity in naive cell cultures, as well as more effective strategies for enrichment of unbiased naive hPSCs. One possible strategy would be sorting cells prior to blastoid generation.

The current study presents limitations. Here, we evaluated XCI using a single X-linked gene. In order to fully understand the XCI status of stem cells and blastoids, it would be necessary to assess multiple genes simultaneously. This could be done by RT-PCR of X-linked SNPs of single cells or high-depth scRNA-seq, for example. Additionally, to our knowledge, even though the WIBR3 MECP2-GFP/tdTomato cell

line used in this work has been previously employed in multiple studies (THEUNISSEN et al, 2016; AN et al., 2020), the half-life of MECP2-tdTomato and MECP2-GFP have not been determined. Therefore, the biallelic MECP2 expression detected could be due to fluorescence from residual proteins. This implies that our experiments provide an upper time limit for XCI, which could actually be happening earlier.

In the future, additional experiments could complement the results obtained in this work. One hypothesis is that only high-tomato cells present in naive cultures are able to undergo random X chromosome inactivation. Therefore, it would be interesting to check if blastoids derived from sorted high-tomato cells present less XCI bias towards the previously inactive allele. Here, we also showed that XCI is heterogenous and incomplete by the 8th day of the blastoid generation protocol. Recently, different conditions for postimplantation-like blastoid culture have been developed (KAGAWA et al., 2022, YU, L. et al., 2022). Extended blastoid culture may provide enough time for XCI completion. In addition, these platforms could be used for simultaneous culture of blastoids and blastocysts, providing a powerful tool to evaluate the suitability of blastoids as models for early human development.

6 - Conclusions

1. Female PSCs in the primed state present monoallelic *MECP2* expression and display a single *XIST* cloud, suggesting activation of a single X chromosome copy;
2. Upon naive conversion, cells present biallelic *MECP2* expression and stop expressing *XIST*, suggesting activation of both X chromosomes;
3. Upon repriming, naive cells cultured in 5iLA tend to inactivate the previously inactive allele;
4. Female EPSCs cultured in LCDM present a low rate of biallelically expressed genes and monoallelic *MECP2* expression, suggesting activation of a single X chromosome copy;
5. Female PSCs cultures in 4CL medium present monoallelic *MECP2* expression, suggesting activation of a single X chromosome copy;
6. Blastoids generated from PXGL cells undergo progressive random XCI, with bias for inactivation of the previously inactive allele. XCI is not complete by the 8th day of protocol.

Figure 14: Diagram summarizing the main findings of this work.

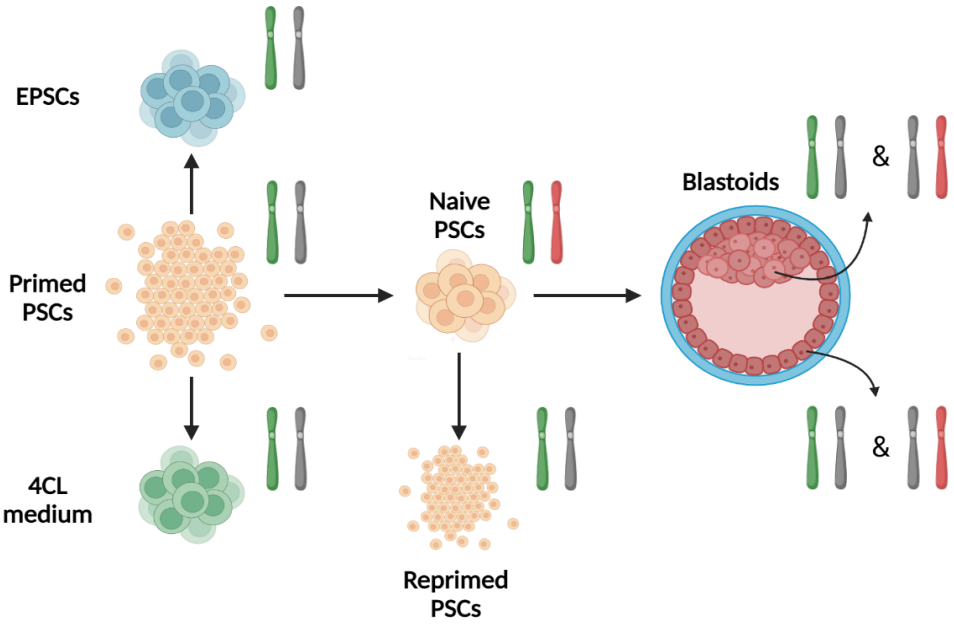

References: this work.

References

AMADEI, G. et al. Synthetic embryos complete gastrulation to neurulation and organogenesis. **Nature**, p. 1–3, 2022.

AMITA, M. et al. Complete and unidirectional conversion of human embryonic stem cells to trophoblast by BMP4. P**roceedings of the National Academy of Sciences**, v. 110, n. 13, p. E1212–E1221, 2013.

AN, C. et al. Overcoming Autocrine FGF Signaling-Induced Heterogeneity in Naive Human ESCs Enables Modeling of Random X Chromosome Inactivation. **Cell Stem Cell**, v. 27, n. 3, p. 482-497.e4, 2020.

BALATON, B. P.; COTTON, A. M.; BROWN, C. J. Derivation of consensus inactivation status for X-linked genes from genome-wide studies. **Biology of Sex Differences,** v. 6, n. 1, 2015.

BARR, M. L.; BERTRAM, E. G. A Morphological Distinction between Neurones of the Male and Female, and the Behaviour of the Nucleolar Satellite during Accelerated Nucleoprotein Synthesis. **Nature**, v. 163, n. 4148, p. 676–677, 1949.

BAYERL, J. et al. Principles of signaling pathway modulation for enhancing human naive pluripotency induction. **Cell Stem Cell**, v. 28, n. 9, p. 1549-1565.e12, 2021.

BERLETCH, J. B. et al. Escape from X Inactivation Varies in Mouse Tissues. **PLOS Genetics**, v. 11, n. 3, p. e1005079, 2015.

BISONG, E. Matplotlib and Seaborn. **Building Machine Learning and Deep Learning Models on Google Cloud Platform**, p. 151–165, 2019.

BOROVIAK, T. et al. The ability of inner-cell-mass cells to self-renew as embryonic stem cells is acquired following epiblast specification. **Nature Cell Biology**, v. 16, n. 6, p. 513–525, 2014.

BREDENKAMP, N. et al. Wnt Inhibition Facilitates RNA-Mediated Reprogramming of Human Somatic Cells to Naive Pluripotency. **Stem Cell Reports**, v. 13, n. 6, p. 1083–1098, 2019.

BRONS, I. G. M. et al. Derivation of pluripotent epiblast stem cells from mammalian embryos. **Nature**, v. 448, n. 7150, p. 191–195, 2007.

BROWN, C. J. et al. Localization of the X inactivation centre on the human X chromosome in Xq13. **Nature**, v. 349, n. 6304, p. 82–84, 1991.

BROWN, C. J. et al. A gene from the region of the human X inactivation centre is expressed exclusively from the inactive X chromosome. **Nature**, v. 349, n. 6304, p. 38–44, 1991.

BROWN, C. J. et al. The human XIST gene: Analysis of a 17 kb inactive X-specific RNA that contains conserved repeats and is highly localized within the nucleus. **Cell**, v. 71, n. 3, p. 527–542, 1992.

CAMPBELL, S. et al. Integrins and adhesion molecules: Cell adhesion molecules on the oocyte and preimplantation human embryo. **Human Reproduction**, v. 10, n. 6, p. 1571–1578, 1995.

CARREL, L. et al. A first-generation X-inactivation profile of the human X chromosome. **Proceedings of the National Academy of Sciences**, v. 96, n. 25, p. 14440–14444, 1999.

CARREL, L.; WILLARD, H. F. X-inactivation profile reveals extensive variability in X-linked gene expression in females. **Nature**, v. 434, n. 7031, p. 400–404, 2005.

CHEN, Y. et al. A versatile polypharmacology platform promotes cytoprotection and viability of human pluripotent and differentiated cells. **Nature Methods**, 2021.

CHUREAU, C. et al. Ftx is a non-coding RNA which affects Xist expression and chromatin structure within the X-inactivation center region. **Human Molecular Genetics,** v. 20, n. 4, p. 705–718, 2010.

COLLIER, A. J.; RUGG-GUNN, P. J. Identifying Human Naïve Pluripotent Stem Cells – Evaluating State-Specific Reporter Lines and Cell-Surface Markers. **BioEssays**, v. 40, n. 5, p. 1700239–1700239, 2018.

COTICCHIO, G. et al. The enigmatic morula: mechanisms of development, cell fate determination, self-correction and implications for ART. **Human Reproduction Update**, v. 25, n. 4, p. 422–438, 2019.

DATTANI, A. et al. Suppression of YAP safeguards human naïve pluripotency. **Development**, v. 149, n. 24, 2022.

DEBRAND, E. et al. Functional Analysis of the DXPas34 Locus, a 3′ Regulator of Xist Expression. **Molecular Cell Biology**, v. 19, n. 12, p. 8513–8525, 1999.

DE LOS ANGELES, A. et al. Hallmarks of pluripotency. **Nature**, v. 525, n. 7570, p. 469–478, 2015.

DENG, X. et al. Evidence for compensatory upregulation of expressed X-linked genes in mammals, Caenorhabditis elegans and Drosophila melanogaster. **Nature Genetics**, v. 43, n. 12, p. 1179–1185, 2011.

DI STEFANO, B. et al. Reduced MEK inhibition preserves genomic stability in naive human embryonic stem cells. **Nature Methods**, v. 15, n. 9, p. 732–740, 2018.

DONOHOE, M. E. et al. The pluripotency factor Oct4 interacts with Ctcf and also controls X-chromosome pairing and counting. **Nature**, v. 460, n. 7251, p. 128–132, 2009.

ECKERT, J. J.; FLEMING, T. P. Tight junction biogenesis during early development. **Biochimica et Biophysica Acta (BBA) - Biomembranes**, v. 1778, n. 3, p. 717–728, 2008.

EGGAN, K. X-Chromosome Inactivation in Cloned Mouse Embryos. **Science**, v. 290, n. 5496, p. 1578–1581, 2000.

EVANS, M. J.; KAUFMAN, M. H. Establishment in culture of pluripotential cells from mouse embryos. **Nature**, v. 292, n. 5819, p. 154–156, 1981.

FAN, Y. et al. Generation of human blastocyst-like structures from pluripotent stem cells. **Cell Discovery**, v. 7, n. 1, 2021.

GAO, X. et al. Establishment of porcine and human expanded potential stem cells. **Nature Cell Biology**, v. 21, n. 6, p. 687–699, 2019.

GENOLET, O. et al. Identification of X-chromosomal genes that drive sex differences in embryonic stem cells through a hierarchical CRISPR screening approach. **Genome Biology**, v. 22, n. 110, 2021.

GERRI, C. et al. Initiation of a conserved trophectoderm program in human, cow and mouse embryos. **Nature**, v. 587, n. 7834, p. 443–447, 2020.

GONTAN, C. et al. RNF12 initiates X-chromosome inactivation by targeting REX1 for degradation. **Nature**, v. 485, n. 7398, p. 386–390, 2012.

GUO, G. et al. Epigenetic resetting of human pluripotency. **Development**, v. 144, n. 15, p. 2748–2763, 2017.

GUO, G. et al. Human naive epiblast cells possess unrestricted lineage potential. **Cell Stem Cell**, v. 28, n. 6, p. 1040-1056.e6, 2021.

HARVEY, K. F.; ZHANG, X.; THOMAS, D. M. The Hippo pathway and human cancer. **Nature Reviews Cancer**, v. 13, n. 4, p. 246–257, 2013.

HEIDARI KHOEI, H. et al. Generating human blastoids modeling blastocyst-stage embryos and implantation. **Nature Protocols**, 2023.

HEMBERGER, M. et al. Parp1-deficiency induces differentiation of ES cells into trophoblast derivatives. **Developmental Biology**, v. 257, n. 2, p. 371–381, 2003.

HUYNH, K. A.; LEE, J. T. Inheritance of a pre-inactivated paternal X chromosome in early mouse embryos. **Nature**, v. 426, n. 6968, p. 857–62, 2003.

JANISZEWSKI, A. et al. Dynamic reversal of random X-Chromosome inactivation during iPSC reprogramming. **Genome Research**, v. 29, n. 10, p. 1659–1672, 2019.

KAGAWA, H. et al. Human blastoids model blastocyst development and implantation. **Nature**, v. 601, n. 7894, p. 600–605, 2022.

KAUR, H.; RV, P.; GAYEN, S. Dampened X-chromosomes in human pluripotent stem cells: dampening or erasure of X-upregulation? **Chromosoma**, v. 129, n. 2, p. 111–113, 2019.

KONO, K.; TAMASHIRO, D. A. A.; ALARCON, V. B. Inhibition of RHO–ROCK signaling enhances ICM and suppresses TE characteristics through activation of Hippo signaling in the mouse blastocyst. **Developmental Biology**, v. 394, n. 1, p. 142–155, 2014.

LARSSON, A. J. M. et al. X-chromosome upregulation is driven by increased burst frequency. **Nature Structural & Molecular Biology**, v. 26, n. 10, p. 963–969, 2019.

LEE, J.; DAVIDOW, L. S.; WARSHAWSKY, D. Tsix, a gene antisense to Xist at the X-inactivation centre. **Nature Genetics**, v. 21, n. 4, p. 400–404, 1999.

LI, R.; ZHONG, C.; IZPISUA BELMONTE, J. C. Time matters: Human blastoids resemble the sequence of blastocyst development. **Cell**, v. 185, n. 4, p. 581–584, 2022.

LINNEBERG-AGERHOLM, M. et al. Naïve human pluripotent stem cells respond to Wnt, Nodal, and LIF signalling to produce expandable naïve extra-embryonic endoderm. **Development**, 2019.

LIU, X. et al. Modelling human blastocysts by reprogramming fibroblasts into iBlastoids. **Nature**, v. 591, n. 7851, p. 627–632, 2021.

LUIJKX, D. et al. From Mice to Men: Generation of Human Blastocyst-Like Structures In Vitro. **Frontiers in Cell and Developmental Biology**, v. 10, 2022.

LYON, M. F. Gene Action in the X-chromosome of the Mouse (Mus musculus L.). **Nature**, v. 190, n. 4773, p. 372–373, 1961.

LYON, M. F. Sex Chromatin and Gene Action in the Mammalian X-Chromosome. **American Journal of Human Genetics**, v. 14, n. 2, p. 135–148, 1962.

LYON, M. F. X-chromosome inactivation. **Current Biology**, v. 9, n. 7, p. R235–R237, 1999.

MAHERALI, N. et al. Directly reprogrammed fibroblasts show global epigenetic remodeling and widespread tissue contribution. **Cell stem cell**, v. 1, n. 1, p. 55–70, 2007.

MAK, W. Reactivation of the Paternal X Chromosome in Early Mouse Embryos. **Science**, v. 303, n. 5658, p. 666–669, 2004.

MANDAL, S. et al. Single-Cell Analysis Reveals Partial Reactivation of X Chromosome instead of Chromosome-wide Dampening in Naive Human Pluripotent Stem Cells. **Stem Cell Reports**, v. 14, n. 5, p. 745–754, 2020.

MARTIN, G. R. Isolation of a pluripotent cell line from early mouse embryos cultured in medium conditioned by teratocarcinoma stem cells. **Proceedings of the National Academy of Sciences**, v. 78, n. 12, p. 7634–7638, 1981.

MAZID, M. A. et al. Rolling back human pluripotent stem cells to an eight-cell embryo-like stage. **Nature**, v. 605, n. 7909, p. 315–324, 2022.

MEKHOUBAD, S. et al. Erosion of Dosage Compensation Impacts Human iPSC Disease Modeling. **Cell Stem Cell**, v. 10, n. 5, p. 595–609,2012

MIHAJLOVIĆ, A. I.; BRUCE, A. W. The first cell-fate decision of mouse preimplantation embryo development: integrating cell position and polarity. **Open Biology**, v. 7, n. 11, p. 170210, 2017.

MINKOVSKY, A. et al. The Pluripotency Factor-Bound Intron 1 of Xist Is Dispensable for X Chromosome Inactivation and Reactivation In Vitro and In Vivo. **Cell Reports**, v. 3, n. 3, p. 905–918, 2013.

MOREIRA DE MELLO, J. C. et al. Random X Inactivation and Extensive Mosaicism in Human Placenta Revealed by Analysis of Allele-Specific Gene Expression along the X Chromosome. **PLoS ONE**, v. 5, n. 6, p. e10947, 2010.

MOREIRA DE MELLO, J. C. et al. Early X chromosome inactivation during human preimplantation development revealed by single-cell RNA-sequencing. **Scientific Reports**, v. 7, n. 1, 2017.

NAVARRO, P. et al. Molecular coupling of Xist regulation and pluripotency. **Science**, v. 321, n. 5896, p. 1693–1695, 2008.

NAZOR, K. L. et al. Recurrent Variations in DNA Methylation in Human Pluripotent Stem Cells and Their Differentiated Derivatives. **Cell Stem Cell**, v. 10, n. 5, p. 620–634, 2012.

NICHOLS, J.; SMITH, A. Naive and Primed Pluripotent States. **Cell Stem Cell**, v. 4, n. 6, p. 487–492, 2009.

NORA, E. P. et al. Spatial partitioning of the regulatory landscape of the X-inactivation centre. **Nature**, v. 485, n. 7398, p. 381–385, 2012.

OGAWA, Y.; LEE, J. T. Xite, X-Inactivation Intergenic Transcription Elements that Regulate the Probability of Choice. **Molecular Cell**, v. 11, n. 3, p. 731–743, 2003.

OHNO, S. Sex Chromosomes and Sex-Linked Genes. [s.l.] **Springer Science & Business Media**, 2013.

OHNO, S.; KAPLAN, W. D.; KINOSITA, R. Formation of the sex chromatin by a single X-chromosome in liver cells of Rattus norvegicus. **Experimental Cell Research**, v. 18, n. 2, p. 415–418, 1959.

OKAE, H. et al. Derivation of Human Trophoblast Stem Cells. **Cell Stem Cell**, v. 22, n. 1, p. 50-63.e6, 2018.

OKAMOTO, I. Epigenetic Dynamics of Imprinted X Inactivation During Early Mouse Development. **Science**, v. 303, n. 5658, p. 644–649, 2004.

OKAMOTO, I. et al. Eutherian mammals use diverse strategies to initiate X-chromosome inactivation during development. **Nature**, v. 472, n. 7343, p. 370–374, 2011.

PARK, W. W. The occurrence of sex chromatin in early human and macaque embryos. **Journal of anatomy**, v. 91, n. 3, p. 369–73, 1957.

PASTOR, W. A. et al. Naive Human Pluripotent Cells Feature a Methylation Landscape Devoid of Blastocyst or Germline Memory. **Cell Stem Cell**, v. 18, n. 3, p. 323–329, 2016.

PAYER, B. et al. Tsix RNA and the Germline Factor, PRDM14, Link X Reactivation and Stem Cell Reprogramming. **Molecular Cell**, v. 52, n. 6, p. 805–818, 2013.

PENNY, G. D. et al. Requirement for Xist in X chromosome inactivation. **Nature**, v. 379, n. 6561, p. 131–137, 1996.

PEREZ-MORENO, M.; JAMORA, C.; FUCHS, E. Sticky Business. **Cell**, v. 112, n. 4, p. 535–548, 2003.

PETROPOULOS, S. et al. Single-Cell RNA-Seq Reveals Lineage and X Chromosome Dynamics in Human Preimplantation Embryos. **Cell**, v. 165, n. 4, p. 1012–1026, 2016.

RASTAN, S.; ROBERTSON, E. J. X-chromosome deletions in embryo-derived (EK) cell lines associated with lack of X-chromosome inactivation. **Development**, v. 90, n. 1, p. 379–388, 1985.

RIETHMACHER, D.; BRINKMANN, V.; BIRCHMEIER, C. A targeted mutation in the mouse E-cadherin gene results in defective preimplantation development. **Proceedings of the National Academy of Sciences**, v. 92, n. 3, p. 855–859, 1995.

RIVRON, N. C. et al. Blastocyst-like structures generated solely from stem cells. **Nature**, v. 557, n. 7703, p. 106–111, 2018.

ROSS, M. T. et al. The DNA sequence of the human X chromosome. **Nature**, v. 434, n. 7031, p. 325–337, 2005.

SAHAKYAN, A. et al. Human Naive Pluripotent Stem Cells Model X Chromosome Dampening and X Inactivation. **Cell Stem Cell**, v. 20, n. 1, p. 87–101, 2017.

SHAHBAZI, M. N. Mechanisms of human embryo development: from cell fate to tissue shape and back. **Development**, v. 147, n. 14, p. dev190629, 2020.

SHEN, Y. et al. X-inactivation in female human embryonic stem cells is in a nonrandom pattern and prone to epigenetic alterations. **Proceedings of the National Academy of Sciences**, v. 105, n. 12, p. 4709–4714, 2008.

SILVA, S. S. et al. X-chromosome inactivation and epigenetic fluidity in human embryonic stem cells. **Proceedings of the National Academy of Sciences**, v. 105, n. 12, p. 4820–4825, 2008.

SOZEN, B. et al. Reconstructing aspects of human embryogenesis with pluripotent stem cells. **Nature Communications**, v. 12, n. 1, p. 5550, 2021.

TAKAHASHI, K.; YAMANAKA, S. Induction of Pluripotent Stem Cells from Mouse Embryonic and Adult Fibroblast Cultures by Defined Factors. **Cell**, v. 126, n. 4, p. 663–676, 2006.

TAKASHIMA, Y. et al. Resetting Transcription Factor Control Circuitry toward Ground-State Pluripotency in Human. **Cell**, v. 158, n. 6, p. 1254–1269, 2014.

TANAKA, S. Promotion of Trophoblast Stem Cell Proliferation by FGF4. **Science**, v. 282, n. 5396, p. 2072–2075, 1998.

TARAZI, S. et al. Post-gastrulation synthetic embryos generated ex utero from mouse naive ESCs. **Cell**, v. 185, n. 18, p. 3290-3306.e25, 2022.

TAUBENSCHMID-STOWERS, J. et al. 8C-like cells capture the human zygotic genome activation program in vitro. **Cell Stem Cell**, v. 29, n. 3, p. 449-459.e6, 2022.

TESAR, P. J. et al. New cell lines from mouse epiblast share defining features with human embryonic stem cells. **Nature**, v. 448, n. 7150, p. 196–199, 2007.

THEUNISSEN, T. W. et al. Systematic Identification of Culture Conditions for Induction and Maintenance of Naive Human Pluripotency. **Cell Stem Cell**, v. 15, n. 4, p. 471–487, 2014.

THEUNISSEN, T. W. et al. Molecular Criteria for Defining the Naive Human Pluripotent State. **Cell Stem Cell**, v. 19, n. 4, p. 502–515, 2016.

THOMSON, J. A. Embryonic Stem Cell Lines Derived from Human Blastocysts. **Science**, v. 282, n. 5391, p. 1145–1147, 1998.

TIAN, D.; SUN, S.; LEE, J. T. The long noncoding RNA, Jpx, is a molecular switch for X chromosome inactivation. **Cell**, v. 143, n. 3, p. 390–403, 2010.

TUKIAINEN, T. et al. Landscape of X chromosome inactivation across human tissues. **Nature**, v. 550, n. 7675, p. 244–248, 2017.

VALLOT, C. et al. XACT, a long noncoding transcript coating the active X chromosome in human pluripotent cells. **Nature Genetics,** v. 45, n. 3, p. 239–241, 2013.

VALLOT, C. et al. XACT Noncoding RNA Competes with XIST in the Control of X Chromosome Activity during Human Early Development. **Cell Stem Cell**, v. 20, n. 1, p. 102–111, 2017.

VESTWEBER, D.; KEMLER, R. Identification of a putative cell adhesion domain of uvomorulin. **The EMBO Journal**, v. 4, n. 13A, p. 3393–3398, 1985.

VESTWEBER, D. et al. Expression and distribution of cell adhesion molecule uvomorulin in mouse preimplantation embryos. **Developmental Biology**, v. 124, n. 2, p. 451–456, 1987.

VIRTANEN, P. et al. SciPy 1.0: fundamental algorithms for scientific computing in Python. **Nature Methods**, v. 17, n. 3, p. 261–272, 2020.

WATSON, A. J.; BARCROFT, L. C. Regulation of blastocyst formation. **Frontiers in bioscience: a journal and virtual library**, v. 6, p. 708–730, 2001.

WUTZ, A.; JAENISCH, R. A Shift from Reversible to Irreversible X Inactivation Is Triggered during ES Cell Differentiation. **Molecular Cell**, v. 5, n. 4, p. 695–705, 2000.

YABE, S. et al. Comparison of syncytiotrophoblast generated from human embryonic stem cells and from term placentas. **Proceedings of the National Academy of Sciences**, v. 113, n. 19, p. E2598–E2607, 2016.

YANAGIDA, A. et al. Naive stem cell blastocyst model captures human embryo lineage segregation. **Cell Stem Cell**, v. 28, n. 6, p. 1016-1022.e4, 2021.

YANG, J. et al. Establishment of mouse expanded potential stem cells. **Nature**, v. 550, n. 7676, p. 393–397, 2017.

YANG, Y. et al. Derivation of Pluripotent Stem Cells with In Vivo Embryonic and Extraembryonic Potency. **Cell**, v. 169, n. 2, p. 243-257.e25, 2017.

YING, Q.-L. et al. The ground state of embryonic stem cell self-renewal. **Nature**, v. 453, n. 7194, p. 519–23, 2008.

YOSHIHARA, M. et al. Transient DUX4 expression in human embryonic stem cells induces blastomere-like expression program that is marked by SLC34A2. **Stem Cell Reports**, v. 17, n. 7, p. 1743–1756, 2022.

YU, L. et al. Blastocyst-like structures generated from human pluripotent stem cells. **Nature**, v. 591, n. 7851, p. 620–626, 2021.

YU, L. et al. Large scale production of human blastoids amenable to modeling blastocyst development and maternal-fetal crosstalk. **bioRxiv**, 2022.

YU, X. et al. Recapitulating early human development with 8C-like cells. **Cell Reports**, v. 39, n. 12, p. 110994, 2022.

ZHAO, C. et al. Reprogrammed blastoids contain amnion-like cells but not trophectoderm. **bioRxiv,** 2021.

ZHENG, R. et al. Derivation of feeder-free human extended pluripotent stem cells. **Stem Cell Reports**, 2021.

ZIMMERLIN, L. et al. Tankyrase inhibition promotes a stable human naïve pluripotent state with improved functionality. **Development**, 2016.

Figures 2 and 14 were created with BioRender.com